nature medicine

Article

https://doi.org/10.1038/s41591-026-04673-3

Urine cell-free RNA for bladder cancer detection and treatment response prediction

Received: 24 February 2026

Accepted: 25 August 2026

Published online: 02 October 2026

Check for updates

A list of authors and their affiliations appears at the end of the paper

Urine biomarkers promise to improve noninvasive detection and molecular characterization of genitourinary malignancies. Here we describe urine random priming and affinity capture of cell-free RNA (cfRNA) fragments for enrichment analysis by sequencing (uRARE-seq), a liquid biopsy method for urine cfRNA profiling, and apply it to 683 urine samples from patients with cancer and controls. Urine cfRNA contained transcripts from genitourinary tissues and, in patients with prostate, kidney or bladder cancer, tumor-derived transcripts. uRARE-seq demonstrated 95% sensitivity at 90% specificity for detecting localized bladder cancer. The method outperformed urine tumor DNA analysis and was unaffected by the presence of field-effect mutations. Urine cfRNA analysis also sensitively detected minimal residual disease and distinguished complete molecular responses after surgery from those after intravesical Bacillus Calmette–Guérin (BCG). Pretreatment urine from complete responders to BCG was enriched for T cell and other immune signatures, suggesting a preexisting antitumor immune response, whereas nonresponders showed higher expression of proliferation-related genes. In pretreatment urine from 114 patients, this biological difference enabled development of a biomarker predicting likelihood of response to BCG versus chemotherapy (area under the curve 0.93) that was strongly associated with risk of recurrence. Urine cfRNA analysis is therefore a promising biomarker approach for bladder cancer and potentially other urologic malignancies, although prospective studies are needed to assess its clinical utility.

The development of improved biomarkers for noninvasive detection and characterization of genitourinary malignancies remains an important goal, especially in bladder cancer (BLCA), given its rising prevalence and resource-intensive surveillance requirements[1]. Urine-based liquid biopsy approaches are attractive, since urine is in direct contact with BLCAs and can be collected noninvasively. Urine cell-free RNA (cfRNA) is a promising analyte, but has not been extensively explored and prior studies mainly focused on the analysis of a small number of genes[2–7]. We hypothesized that broader expression profiling of urine cfRNA using high-throughput sequencing would allow sensitive and specific detection of tumor-derived transcripts. Here we report the development of a urine cfRNA sequencing method called urine random priming and affinity capture of cfRNA fragments for enrichment analysis by sequencing (uRARE-seq) and characterize its performance for noninvasive BLCA detection and molecular characterization.

Results

Analysis of urine cfRNA

In contrast to RNA from cellular urinary sediments, cfRNA from urinary supernatants is highly fragmented (Extended Data Fig. 1a), suggesting that a sequencing approach optimized for short RNA fragments would be required. We therefore adapted RARE-Seq[8], a hybrid capture-based sequencing approach for plasma cfRNA, to analyze urine cfRNA. We compared three extraction strategies

e-mail: arasha@stanford.edu; jliao@stanford.edu; diehn@stanford.edu

https://doi.org/10.1038/s41591-026-04673-3

and found that a silica column-based approach yielded the highest RNA concentrations (Extended Data Fig. 1b). Urine specific gravity was significantly correlated with RNA yield ($R = 0.5$, $P = 0.0004$; Extended Data Fig. 1c), but did not impact gene expression profiles (Extended Data Fig. 1d). RNA yield was inversely associated with urine pH, consistent with lower RNA stability under alkaline conditions ($P = 0.002$; Extended Data Fig. 1e) but unaffected by storage time at −80 °C ($R = -0.0075$, $P = 0.85$; Extended Data Fig. 1f). Two preservative strategies (ethylenediaminetetraacetic acid or a commercial preservative solution) yielded similar RNA concentrations, fragment sizes and gene expression profiles ($P = 0.66$; Extended Data Fig. 1g,h and Supplementary Table 1). In addition, we observed no significant changes in RNA concentration or transcript abundances after one freeze–thaw cycle (Extended Data Fig. 1i,j). Lastly, to test the stability of urine cfRNA, we compared yield and transcript abundances in samples processed at various time points between 0 and 48 hours after collection. Both cfRNA concentration and gene expression were stable over this timeframe (Extended Data Fig. 1k,l). We refer to the optimized method as uRARE-seq (Fig. 1a).

https://doi.org/10.1038/s41591-026-04673-3

Fig. 1 | Development and application of uRARE-seq for urine cfRNA analysis. **a**, Schematic of the uRARE-seq workflow. **b**, CIBERSORTx[60] gene expression deconvolution using epithelial and hematopoietic genes in paired control urine cfRNA and sediment samples ($n = 5$). **c**, Expression of gene signatures overexpressed in normal tissues in male ($n = 31$) and female ($n = 17$) healthy control urine cfRNA samples. Comparisons were performed using two-sided Student's *t* test. Blue *P* value indicates comparison between male samples and pink *P* value represents comparison between female samples. $^{****}P \leq 2.2 \times 10^{-16}$. **d**, Principal component analysis of whole transcriptome uRARE-seq data using urine samples from BLCA ($n = 20$), RCC ($n = 20$) and PRAD ($n = 20$) patients. **e**, Heatmap of urine cfRNA centered $\log_2$-transformed trimmed mean of M-values (TMM) gene expression values for genes known to be overexpressed in BLCA ($n = 20$), RCC ($n = 20$) or PRAD ($n = 20$) tumors. **f**,**g**,**h**, Hallmark gene set enrichment analysis of **f**, control ($n = 48$) versus BLCA ($n = 20$) urine cfRNA, **g**, control ($n = 48$) versus RCC ($n = 20$) urine cfRNA, and **h**, control ($n = 48$) versus PRAD ($n = 20$) urine cfRNA. Gene sets with adjusted *P* values ≤ 0.05 calculated using Benjamini–Hochberg (BH) multiple hypothesis correction are shown. **i**, Schematic of the process for defining uRAGs. **j**, Percentage of genes overexpressed in GU tumors that are included among uRAGs. Cancer-enriched genes were selected as defined in Methods. Comparisons were performed using two-sided Fisher's exact test. $^{****}P = 0.00001$. **k**, Comparison of unique sequencing depth for shared genes in uRARE-seq libraries captured with both whole-coding transcriptome and uRAG capture panels ($n = 38$ biological samples). Sequencing data were downsampled to achieve equivalent sequencing depth in all samples. Comparison was performed using paired two-sided Student's *t* test. $^{****}P < 2.2 \times 10^{-16}$. In box plots, the center line denotes the median, the box contains the interquartile range (IQR) and the whiskers extend to 1.5× IQR. EMT, epithelial–mesenchymal transition; IFN, interferon; IL, interleukin; JAK, Janus kinase; MTOR, mechanistic target of rapamycin; NF-κB, nuclear factor kappa-light-chain-enhancer of activated B cells; STAT, signal transducer and activator of transcription; TNF, tumor necrosis factor; KIRC, kidney renal clear cell carcinoma. Panels created in BioRender: **a**, Shi, W. https://biorender.com/8nr5ri4 (2026); **i**, Shi, W. https://biorender.com/kk01zkl (2026).

Applying uRARE-seq with a whole-coding transcriptome panel to urinary supernatant and sediment from healthy adults and patients with BLCA, we found urine cfRNA to be highly enriched for epithelial RNA (Fig. 1b and Extended Data Fig. 1m) while urinary sediment RNA was mostly derived from hematopoietic cells (Fig. 1b and Extended Data Fig. 1m). Furthermore, uRARE-seq analysis of urine from 48 healthy controls showed that urine cfRNA primarily contains transcripts from bladder, kidney and prostate and low expression of transcripts from nongenitourinary tissues (Fig. 1c). Highlighting the specificity of our approach, we observed prostate gene expression in males but not females (Fig. 1c). In contrast, genitourinary (GU) transcripts were largely absent from plasma cfRNA samples of 47 healthy controls[8] (Extended Data Fig. 1n–p and Methods). Thus, urine cfRNA analysis enables noninvasive characterization of transcripts from GU tissues.

Urine cfRNA contains transcripts from GU tumors

Next, we analyzed urine cfRNA samples from patients with localized BLCA ($n = 20$), renal cell carcinoma (RCC; $n = 20$) or prostate adenocarcinoma (PRAD; $n = 20$; Supplementary Table 1) and found them to be transcriptionally distinct (Fig. 1d). Furthermore, genes known to be highly expressed in each tumor type such as *IGF2*[9–11], *CRH*[9], *ANXA10*[9], *KRT5*[12] and *KRT14*[13] for BLCA, solute carrier genes (SLCs)[14], *NAT8*[15,16] and *ACSM2A/2B*[15,17] for RCC, and *AR*[18], *KLK2*[18,19], *KLK3* (PSA)[19], *FOLH1* (PSMA)[20] and *TGM4*[20] for PRAD were congruently differentially expressed in urine (Fig. 1e). Gene set enrichment analysis (GSEA) revealed that urine cfRNA from the three cancer types was enriched for distinct gene sets compared to healthy controls, such as hypoxia genes in RCC and androgen response genes in PRAD (Fig. 1f–h).

Identifying urine rare abundance genes for targeted capture

Targeting transcripts that are absent or lowly expressed in plasma cfRNA from healthy individuals increases the sensitivity for detecting cancer-derived transcripts relative to whole-coding transcriptome capture[8]. We therefore hypothesized that a similar strategy could improve GU cancer detection. Applying uRARE-seq to profile whole transcriptomes in urine from 38 noncancer controls, we identified 3,834 urine rare abundance genes (uRAGs) and designed a custom capture panel targeting them (Fig. 1i, Extended Data Fig. 2a, Methods and Supplementary Tables 1 and 2). Although not part of the filtering criteria, the majority of genes specifically overexpressed in GU tumors were included among uRAGs (Fig. 1j and Methods). We supplemented the panel with housekeeping genes ($n = 50$; Extended Data Fig. 2b), genes that are recurrently mutated or have aberrant expression in GU tumors, normal tissue-specific transcripts, and genes to enable immune cell deconvolution (Extended Data Fig. 2c and Methods), bringing the total to 4,782 genes (Supplementary Table 3). Profiling control samples ($n = 38$) using both the whole-coding transcriptome and uRAG capture panels, we observed high correlation of shared genes (Extended Data Fig. 2d; $R = 0.99$; $P < 2.2 \times 10^{-16}$), while the uRAG panel achieved higher unique sequencing depth and detected more genes (Fig. 1k and Extended Data Fig. 2e).

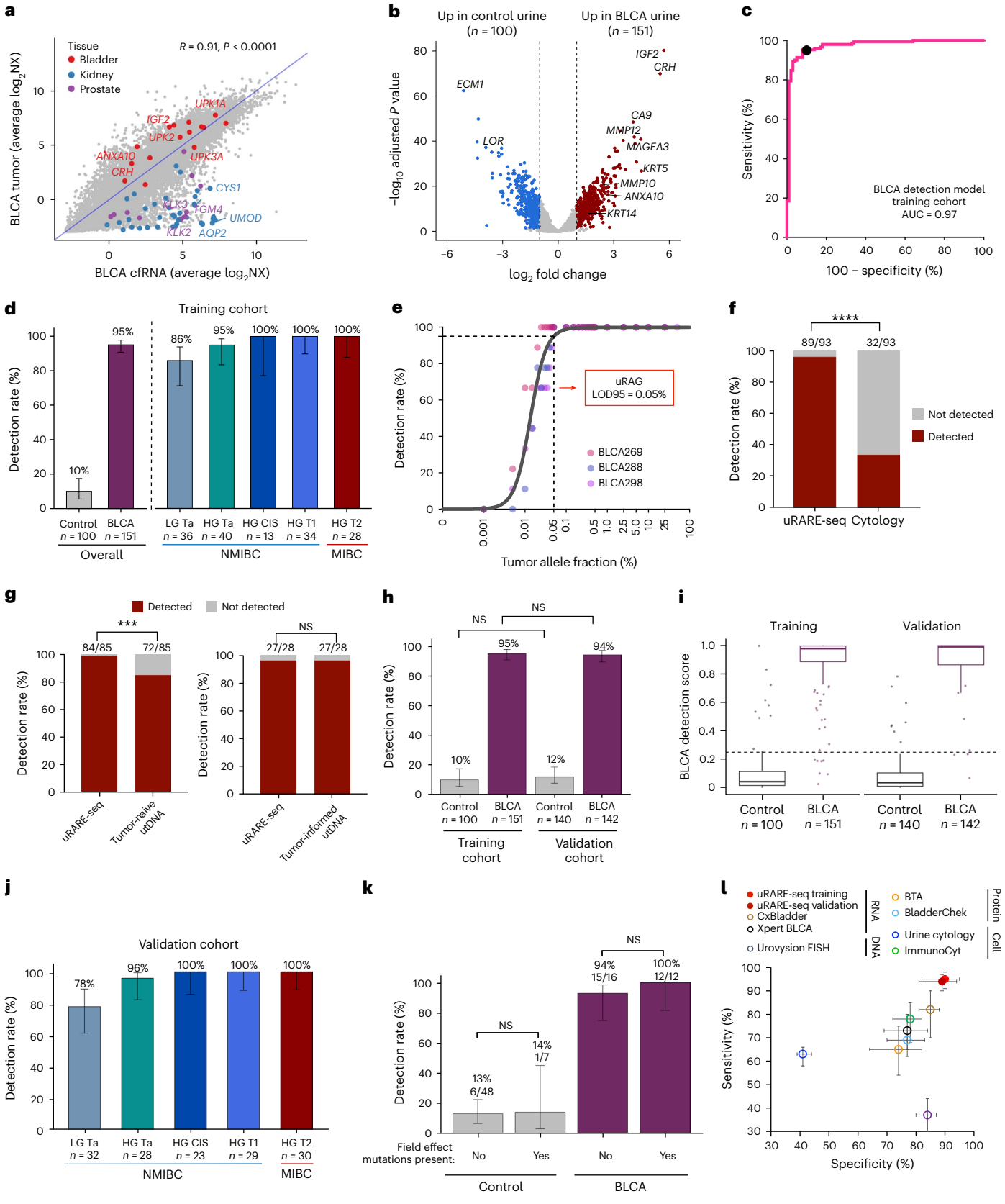
Urine cfRNA gene expression in patients with BLCA and noncancer controls

To demonstrate the potential utility of urine cfRNA analysis, we focused the remainder of our study on localized BLCA. Analyzing matched BLCA tumor tissue and pretreatment urine cfRNA samples, we found the two to be highly correlated ($R = 0.91$; $P < 0.0001$; Fig. 2a). Next, we applied

Fig. 2 | Pretreatment BLCA detection using uRARE-seq. **a**, Correlation between matched BLCA tumor RNA and urine cfRNA ($n = 46$). Colored dots indicate tissue-specific genes. **b**, Differential expression analysis using uRARE-seq data from 100 control and 151 BLCA urine cfRNA samples. Adjusted *P* values indicate BH multiple hypothesis correction. **c**, Receiver operating characteristic (ROC) curve for BLCA detection model in training cohort (100 control and 151 BLCA urine cfRNA samples). Circle indicates 90% specificity. **d**, Cross-validated performance (10-fold) of the elastic net-based BLCA detection model in the training cohort, stratified by tumor grade and stage. Error bars indicate 95% binomial confidence intervals. **e**, Spiking experiment using BLCA ($n = 3$) and control urine ($n = 3$) samples to determine LOD95 (Methods). The presence of BLCA was determined in each spike using the BLCA detection model. Logistic regression was used to estimate the LOD95 (shown as dashed line). **f**, Percent of patients detected by uRARE-seq or urine cytology in samples with both available ($n = 93$). Comparison was performed using two-sided Fisher's exact test. $P = 4.5 \times 10^{-20}$. **g**, Percent of pretreatment samples detected by uRARE-seq and tumor-naive uCAPP-Seq ($n = 85$), or uRARE-seq and tumor-informed/field-effect-informed uCAPP-Seq ($n = 28$) in matched BLCA cases. Specificity was 87% for all assays in a set of 55 controls. Comparisons were performed using two-sided Fisher's exact test. $^{***}P = 0.0005$. **h**, Performance of the validation cohort using the same cutoff set in the training cohort. Comparisons were performed using Fisher's exact test. Error bars indicate 95% binomial confidence intervals. **i**, BLCA detection scores in training ($n = 251$) and validation cohorts ($n = 282$). The dashed line indicates the locked detection threshold based on the training cohort. **j**, Sensitivity of BLCA detection in the validation cohort stratified by grade and stage. Detection threshold based on the locked training cohort 90% specificity was used. Error bars indicate 95% binomial confidence intervals. **k**, Percent of control ($n = 55$) and BLCA ($n = 28$) urine samples called positive using the BLCA detection model based on the presence or absence of field-effect mutations as determined by uCAPP-Seq[27]. Error bars indicate 95% binomial confidence intervals. **l**, Cross-study comparison of sensitivity and specificity for uRARE-seq and clinically available urine BLCA detection tests. Data for the other assays were obtained from literature[2,3,5,7,28,29]. Error bars indicate 95% binomial confidence intervals. In box plots, the center line denotes the median, the box contains the IQR and the whiskers extend to 1.5× IQR. BTA, bladder tumor antigen; NS, not significant.

https://doi.org/10.1038/s41591-026-04673-3

uRARE-seq using the uRAG panel to urine cfRNA from a training cohort of noncancer controls ($n = 100$; 48 asymptomatic and 52 with hematuria or lower urinary symptoms) and pretreatment BLCA urine cfRNA (non-muscle invasive bladder cancer (NMIBC) = 123; muscle-invasive bladder cancer (MIBC) = 28) samples (Extended Data Table 1). Concentrations of cfRNA and sequencing parameters were similar between groups (Extended Data Fig. 3a–c). Differential gene expression analysis identified 3,383 genes, including genes known to be highly expressed in BLCA (Fig. 2b). Genes overexpressed in BLCA urine cfRNA were also highly expressed in BLCA tumor tissues ($P < 0.0001$; Extended Data Fig. 3d).



Urine cfRNA-based detection of BLCA

Next, we applied machine learning to develop a tumor-naive BLCA detection model using uRARE-seq data generated with the uRAG selector (Fig. 2c, Extended Data Fig. 3e, Methods and Supplementary Table 4). To minimize the risk of overfitting, we preselected a subset of 1,066 genes that are differentially expressed between unrelated BLCA tumors and held-out urine cfRNA control samples ($n = 38$) and not associated with sex or hematopoietic cell types (Methods and Extended Data Fig. 3e). The model selected 381 of these genes, including transcripts known to be highly expressed in BLCA such as *IGF2*[9–11], *CRH*[9], *MMPs*[21,22] and *ANXA10*[9]. Across the 251 urine samples in the training cohort, the model achieved an area under the curve (AUC) of 0.97, with a sensitivity of 95% at 90% specificity (Fig. 2c,d). Sensitivity was high across all tumor grades and stages, including 86% in low-grade (LG) Ta (31 of 36), 95% in high-grade (HG) Ta (38 of 40), 100% in carcinoma in situ (13 of 13), 100% in HG T1 (34 of 34), and 100% in HG T2 (28 of 28) (Fig. 2d). Detection was not associated with RNA concentration, RNA input, sequencing depth or sex (Extended Data Fig. 3a–c,f,g), and results were highly reproducible among technical replicates (Extended Data Fig. 3h–k). Subsampling analysis showed stable performance when at least 60% of training cohort samples were included ($n = 151$; Extended Data Fig. 3l). In silico spiking experiments determined the analytical limit of detection at which the BLCA detection model detects 95% of replicates (95% limit of detection; LOD95) to be 0.05% (Fig. 2e and Methods).

We next compared the performance of the BLCA detection model with other urine-based assays. Although urine cytology is commonly performed clinically, its sensitivity is modest, especially for LG tumors[23–25]. Analyzing 93 paired samples, uRARE-seq detected 89 cases (95.7%) and urine cytology detected 32 (34.4%), an absolute difference of 61.3%. Cytology detected no low-grade Ta tumors while uRARE-seq detected 90% (28 of 31; $P < 0.0001$; Fig. 2f, Extended Data Fig. 3m and Supplementary Table 5). Next, we compared performance of uRARE-seq with a tumor-naive urine tumor DNA (utDNA) assay[26] ($n = 85$) and a field-effect- and tumor-informed utDNA assay[27] ($n = 28$) in matched urine samples. The BLCA detection model demonstrated higher sensitivity than the tumor-naive utDNA method (99% versus 85%, $P < 0.001$) and similar sensitivity as the tumor-informed approach (96% for both; Fig. 2g and Supplementary Table 5).

Applying the locked model to an independent validation cohort of pretreatment urine samples from patients with BLCA ($n = 142$) and noncancer controls ($n = 140$) yielded nearly identical performance as in the training cohort (Fig. 2h–j and Extended Data Fig. 3e). Specificity also was high in controls with benign urologic conditions (Extended Data Fig. 3n). Furthermore, in a subset of 55 control and 28 BLCA urine samples that had been evaluated for the presence of field-effect mutations (which negatively impact specificity of utDNA-based methods[27]), performance of uRARE-seq was similar regardless of the presence of field-effect mutations (Fig. 2k and Methods). Finally, the performance of the BLCA detection model was better than the performance reported in studies of several other urine-based BLCA biomarkers (Fig. 2l)[2,3,5,7,28,29].

Grade and muscle invasion can be distinguished using urine cfRNA

We next asked whether uRAG-targeted cfRNA profiling could distinguish LG versus HG and NMIBC versus MIBC (Fig. 3a). Genes enriched in urine cfRNA from patients with LG versus HG NMIBC overlapped significantly with genes differentially expressed in LG versus HG NMIBC tumor tissue[30] ($P < 0.001$; Fig. 3b, Extended Data Fig. 4a and Methods). An elastic net machine learning model trained to predict the likelihood of a patient having HG BLCA ('BLCA grade model'; Fig. 3a, Methods and Supplementary Table 4) achieved an AUC of 0.84 with 10-fold cross-validation in the training cohort and an AUC of 0.84 in the independent validation cohort (Fig. 3c), showed no significant association with potential sources of bias such as cfRNA concentration, input and the number of sequencing reads (Extended Data Fig. 4b–d), and was well calibrated (Extended Data Fig. 4e). Interestingly, among tumors that were clinically annotated as LG, patients with higher BLCA grade model scores were more likely to develop recurrence, suggesting the model is able to detect prognostic features beyond histologic grade (Fig. 3d and Extended Data Fig. 4f,g).

A urine biomarker distinguishing NMIBC from MIBC could help identify patients with NMIBC who are understaged. MIBC urine cfRNA was enriched for basal urothelial markers while NMIBC urine was enriched for luminal markers (Fig. 3e and Extended Data Fig. 4h), and genes that were enriched in NMIBC versus MIBC were similarly enriched in tumor tissue (Extended Data Fig. 4i). A machine learning model trained to predict MIBC ('BLCA muscle invasion model'; Fig. 3a, Methods and Supplementary Table 4) achieved an AUC of 0.82 using 10-fold cross-validation in the training cohort and 0.75 in the independent validation cohort (Fig. 3f). RNA concentration, library input and sequencing reads were similar between the two groups (Extended Data Fig. 4j-l) and the model was well calibrated (Extended Data Fig. 4m).

Detection of minimal residual disease using urine cfRNA

We next tested whether uRAG-targeted uRARE-seq can detect minimal residual disease (MRD) after treatment. We analyzed a cohort of patients with intermediate- and high-risk NMIBC ($n = 36$) undergoing surgery followed by adjuvant Bacillus Calmette–Guérin (BCG) immunotherapy induction, using the locked BLCA detection model. Urine samples collected before surgery ('presurgery'), before BCG induction ('pre-BCG') and at the first follow-up visit ('post-BCG'; Fig. 4a) were analyzed for the presence of BLCA transcripts at each timepoint. Among patients without recurrence, all had detectable BLCA cfRNA presurgery, 58% pre-BCG and none post-BCG, suggesting a subset of patients may have been cured by surgery and the remainder by adjuvant BCG. In contrast, among patients who developed HG recurrence, all had detectable tumor cfRNA both presurgery and pre-BCG, and 92% had detectable tumor cfRNA after BCG (Fig. 4b and Extended Data Fig. 5a, b). CfRNA-positive cases had significantly worse HG recurrence-free survival at both the pre-BCG (HR = 4.30; log-rank $P = 0.02$) (Fig. 4c) and post-BCG (HR = 41.17; log-rank $P < 0.0001$) time points (Fig. 4d). Finally, uRARE-seq detected more patients with recurrence than tumor-naive or tumor-informed utDNA analysis (Extended Data Fig. 5c–f).

Identification of responders to surgery or BCG

Urine cfRNA analysis allows distinguishing patients who have complete molecular responses to surgery from those who have incomplete responses to surgery but then respond to adjuvant BCG. We used the BLCA detection model to classify patients who had undetectable BLCA cfRNA in their postsurgery sample as achieving molecular complete response (mCR after surgery; $n = 10$) and those with residual BLCA cfRNA as having molecular residual disease (mRD after surgery; $n = 26$). We further stratified the latter into two groups: 'mCR after BCG' if they had undetectable BLCA detection scores in the post-BCG sample ($n = 15$) or 'mRD' if they had detectable tumor cfRNA after BCG ($n = 11$; Fig. 5a,b and Methods). The cfRNA response groups were strongly associated with clinical outcomes, with patients having complete molecular responses to either surgery or BCG having much lower risks of recurrence than those with residual BLCA cfRNA after treatment ($P < 0.0001$; Fig. 5c). For a subset of patients with sufficient urine available, utDNA analysis using tumor-informed urine cancer personalized profiling by deep sequencing (uCAPP-Seq)[27] was performed on the same urine samples used for cfRNA analysis ($n = 28$; Extended Data Fig. 6a,b).

Transcriptomic features of BCG responders

Establishing reproducible molecular predictors of a BCG response has proven challenging, in part due to the inability to distinguish

https://doi.org/10.1038/s41591-026-04673-3

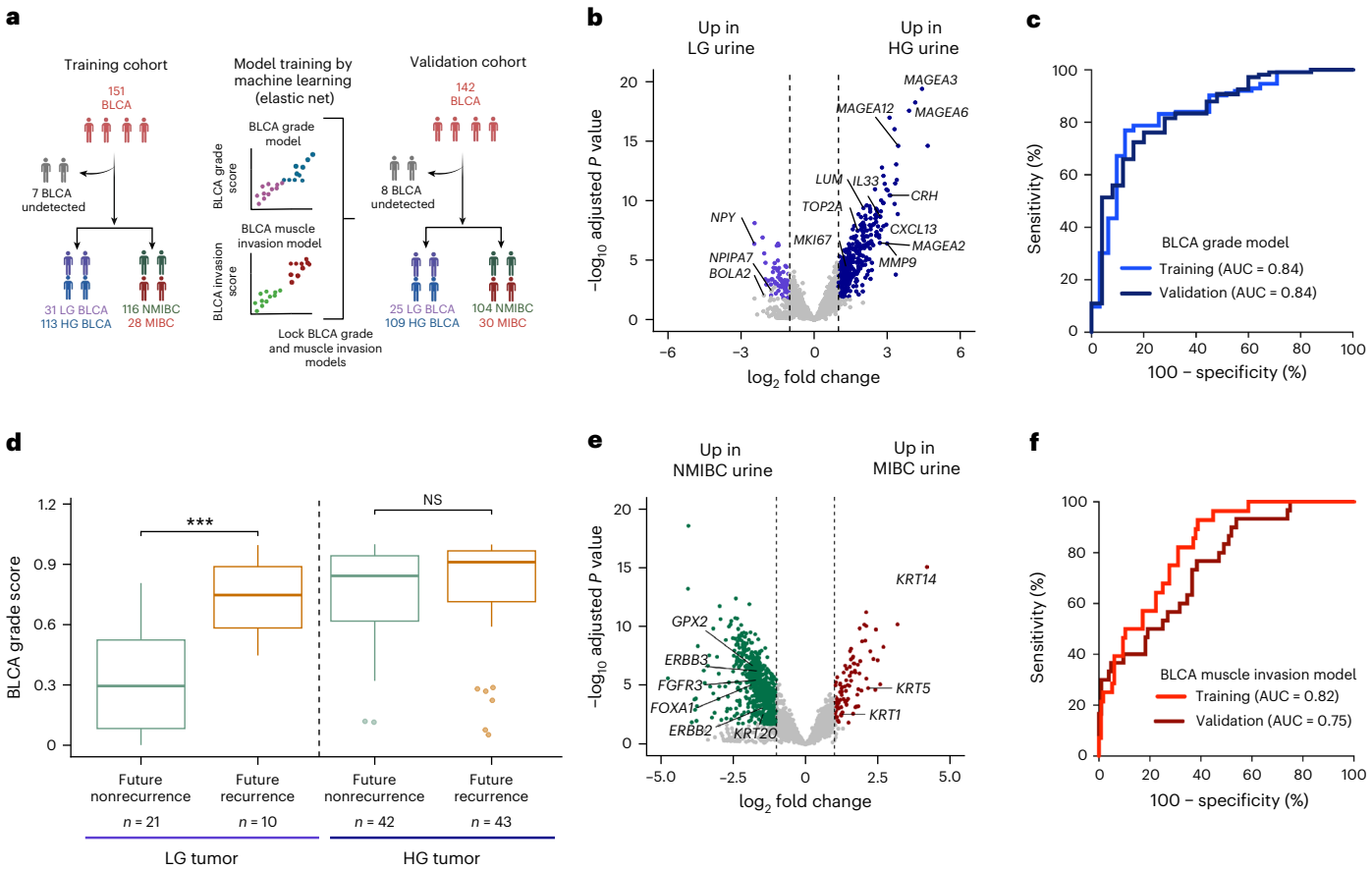


Fig. 3 | Urine-based detection of BLCA grade and invasiveness. a, Schematic for training and validating the BLCA grade and muscle invasion models. **b**, Differential expression analysis between LG ($n = 31$) and HG urine cfRNA ($n = 113$) samples. Adjusted P values indicate BH multiple hypothesis correction. **c**, ROC curves for BLCA grade model in training (31 LG and 113 HG patients) and validation (25 LG and 109 HG patients) cohorts. Ten-fold cross-validation was used in the training cohort. **d**, Case-level uRARE-seq BLCA grade model scores. LG and HG annotation is based on pathologist annotations. Comparisons were performed using two-sided Student's t test. ***$P = 0.0003$; $P > 0.05$, NS. **e**, Differential expression analysis between NMIBC ($n = 116$) and MIBC urine cfRNA ($n = 28$). Adjusted P values indicate BH multiple hypothesis correction. **f**, ROC curves for BLCA muscle invasion model in training (116 patients with NMIBC and 28 with MIBC) and validation (104 patients with NMIBC and 30 with MIBC) cohorts. Ten-fold cross-validation was used in the training cohort. In box plots, the center line denotes the median, the box contains the IQR and the whiskers extend to 1.5× IQR. Panel **a** created in BioRender; Shi, W. https://biorender.com/o500uvu (2026).

accurately between patients who are cured by surgery versus BCG[31,32]. Leveraging the ability of urine cfRNA analysis to disentangle complete responses to surgery versus BCG, we were able to identify transcriptomic features associated with response to each treatment. To do so, we profiled whole-coding transcriptomes in preoperative urine cfRNA specimens of the 26 patients with the samples available from the three landmark time points (Fig. 5a). Thousands of genes were differentially expressed between patients with mCR versus mRD after surgery or BCG (Extended Data Fig. 6c,d). GSEA revealed that patients with mRD after surgery had increased urine cfRNA expression of cancer-related pathways (for example epithelial–mesenchymal transition, glycolysis and angiogenesis) compared to patients who had mCR after surgery (Fig. 5d and Extended Data Fig. 6c).

In contrast, patients with mRD after BCG predominantly had increased expression of proliferation-related signaling pathways such as mitotic spindle and G2M checkpoint genes. Patients with mCR to BCG demonstrated increased expression of immune-related signaling pathways such as tumor necrosis factor signaling, interferon response, inflammatory response, allograft rejection, interleukin 6–Janus kinase–signal transducer and activator of transcription 3 signaling and complement gene sets (Fig. 5e,f and Extended Data Fig. 6d). A previously defined interferon gamma gene expression profile that is associated with response to programmed cell death protein 1 immune checkpoint blockers in multiple solid tumors[33] was also associated with mCR after BCG immunotherapy, but not after surgery (Fig. 5f, Extended Data Fig. 6e and Supplementary Table 6). Additionally, we found that BCG response was associated with expression of T cell transcripts included in a previously defined gene expression metric associated with response to checkpoint inhibitors in urothelial cancers[33–37] (Fig. 5f, Extended Data Fig. 6e and Supplementary Table 6).

Urine cfRNA from responders to adjuvant BCG was also enriched for previously published gene signatures associated with tumor-reactive CD4 and CD8 T cells[38–40], tissue-resident memory T cells[41,42], tertiary lymphoid structures[43], major histocompatibility complex class I[44], and antigen processing and presentation machinery[45] (Fig. 5f and Extended Data Fig. 6e). Conversely, we observed that urine cfRNA from patients who had mRD after adjuvant BCG was enriched for genes associated with cold tumors[36] (Fig. 5f and Extended Data Fig. 6e). T cell receptor repertoire analysis in urine cfRNA revealed that patients who responded to BCG had more T cell clones and a more diverse repertoire compared to patients who did not respond to BCG (Fig. 5g,h). This difference was not observed between patients with and without mCR after surgery (Extended Data Fig. 6f,g). Finally, previously developed tumor gene expression-based classification systems for NMIBC[30,46] were not statistically significantly associated with mCR after surgery or BCG (Extended Data Fig. 6h–k). Collectively, these observations

https://doi.org/10.1038/s41591-026-04673-3

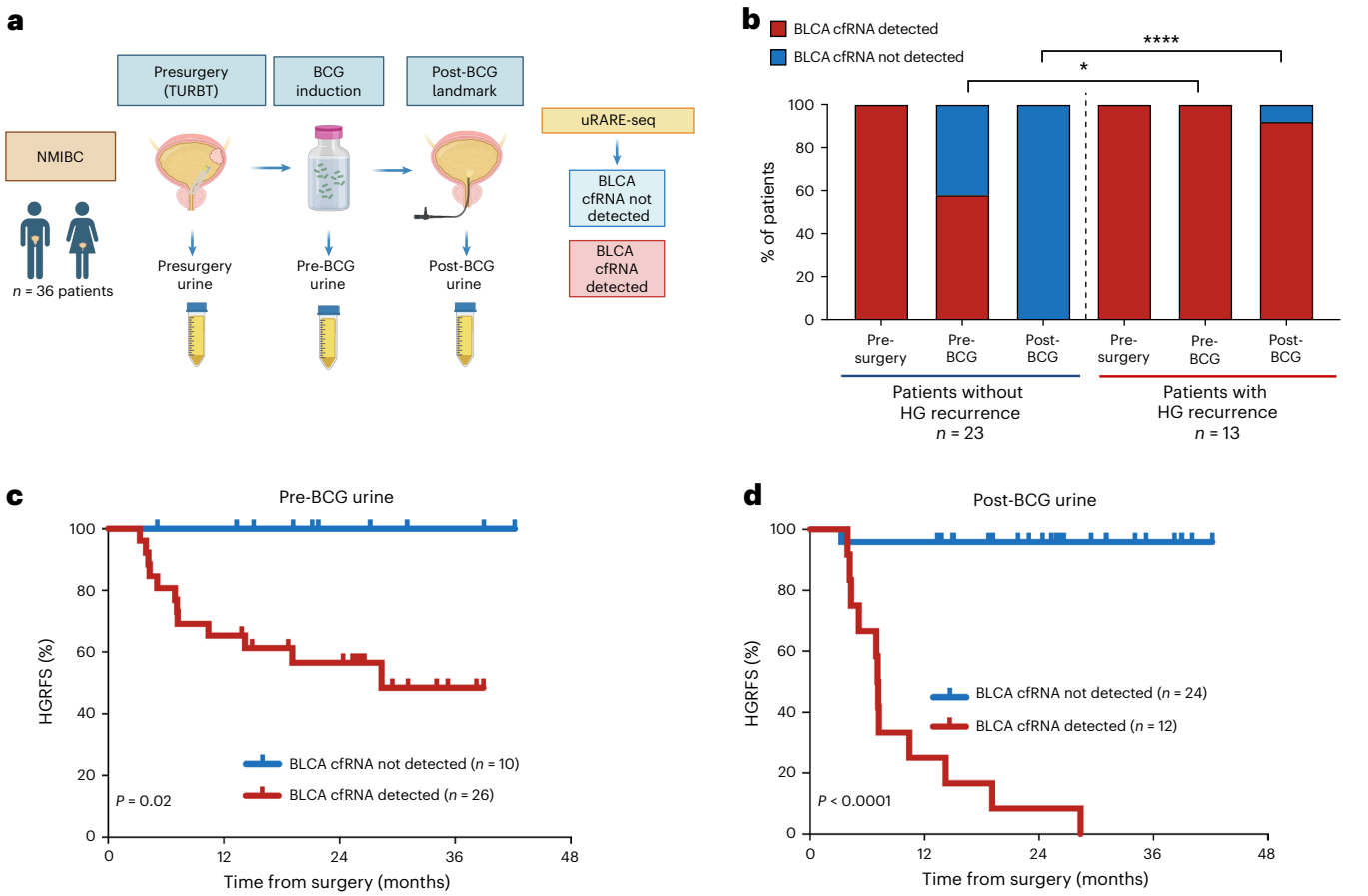


Fig. 4 | MRD detection in NMIBC using uRARE-seq. a, Schematic of BLCA urine collections in a cohort of 36 patients with NMIBC undergoing surgery (transurethral resection of bladder tumor) plus BCG treatment. **b**, Relationship between BLCA detection and patient outcomes at the three landmark time points (presurgery, pre-BCG and post-BCG) stratified by recurrence status. The BLCA detection model was used to determine the presence of BLCA cfRNA. Comparisons were performed using two-sided Fisher's exact test. *P = 0.01; ****P = 0.00001. **c**, Kaplan–Meier analyses stratified by BLCA detection model result in pre-BCG urine cfRNA samples (n = 36). Statistical significance was determined using a two-sided log-rank test. **d**, The same as in **c** but using post-BCG urine samples (n = 36). ****$P = 7.24 \times 10^{-8}$. HGRFS, high-grade recurrence-free survival; TURBT, transurethral resection of bladder tumor. Panel **a** created in BioRender; Shi, W. https://biorender.com/91fbkee (2026).

suggest that the presence of a preexisting antitumor immune response is likely necessary for BCG to be effective.

Predicting responses to adjuvant BCG and chemotherapy

To develop a biomarker predicting BCG response, we trained an 'intravesical therapy response prediction model' using presurgery whole-coding transcriptome urine cfRNA expression data from patients with and without mCR after BCG. We only included genes that were part of immune and proliferation pathways since these were the most striking and coherent biological differences we had observed between responders and nonresponders to BCG (Methods, Fig. 6a and Supplementary Table 4). Using leave-one-out cross-validation, the model achieved an AUC of 0.93, with higher model scores being associated with mCR after BCG (Fig. 6b,c, Supplementary Table 7 and Extended Data Fig. 7a), but not with mCR after surgery (P = 0.4273; Fig. 6d). Scores were also strongly associated with risk of recurrence (Fig. 6e,f). Scores from the locked model were strongly associated with recurrence in an independent validation cohort of patients with NMIBC who underwent surgery followed by BCG induction (n = 57; P = 0.0005; Fig. 6g,h).

Finally, because pretreatment urine from patients with poor BCG responses was enriched for proliferation-related transcripts (Fig. 5e), we wondered if they might be more likely to respond to chemotherapy. We therefore applied the locked intravesical therapy response prediction model to an independent cohort of 38 patients with NMIBC who received intravesical chemotherapy (Fig. 6a). Strikingly, we found that patients who did not develop recurrence had low intravesical therapy response prediction scores while patients who developed recurrence had high scores (P < 0.0001; Fig. 6i,j). These results suggest that urine cfRNA analysis could potentially be used to select the most effective intravesical adjuvant therapy for patients with NMIBC (Fig. 6k).

Discussion

In this study, we introduced uRARE-seq, a tumor-naive method for sensitive analysis of urine cfRNA that can noninvasively detect transcripts stemming from normal genitourinary tissues and malignancies. In patients with BLCA, uRARE-seq enabled highly sensitive cancer detection, discrimination of clinically relevant features such as grade and muscle invasion, and the ability to predict the likelihood of benefit from adjuvant intravesical BCG immunotherapy versus chemotherapy.

A key feature of uRARE-seq is the ability to perform single-sample classification without the need for matched tumor tissue or additional urine samples. The BLCA detection model achieved a pretreatment sensitivity of 95% at 90% specificity and was validated in an independent validation cohort. Our approach demonstrated higher sensitivity for pretreatment detection than both cytology and tumor-naive utDNA analysis, while achieving similarly high performance as a targeted tumor-informed utDNA approach. In future studies, it will be interesting to compare uRARE-seq with ultrasensitive tumor-informed cell-free DNA assays[47,48].

https://doi.org/10.1038/s41591-026-04673-3

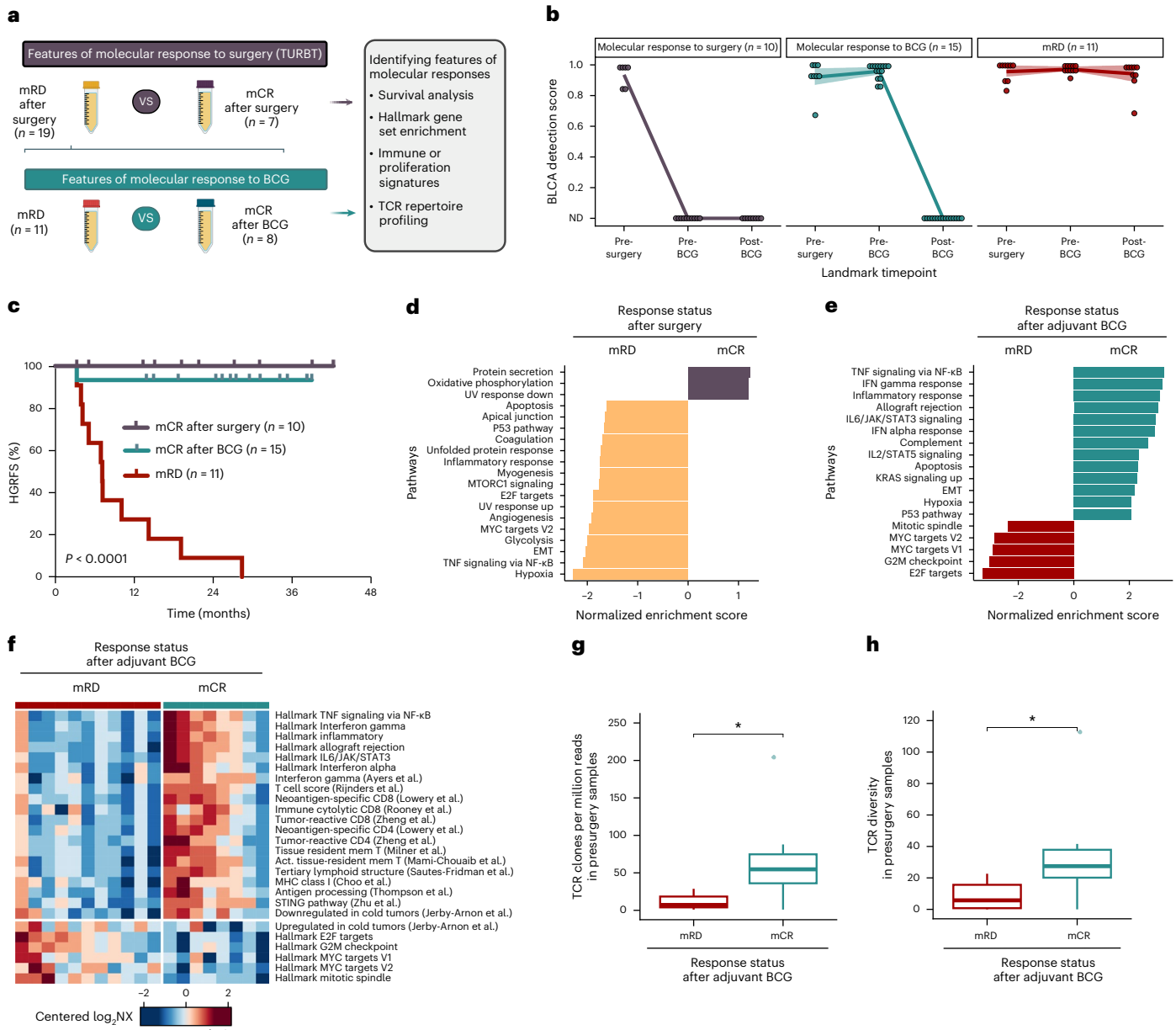


Fig. 5 | Responders to surgery and BCG have distinct cfRNA profiles. **a**, Schematic of the approach used to identify expression-based features of surgery or BCG response. **b**, Sample-level BLCA detection scores grouped by type of molecular response. Lines represent the mean score for each BCG response category and ribbons represent the 95% confidence intervals. **c**, Kaplan–Meier analysis of patients with BLCA stratified by BCG molecular response using the BLCA detection score. Comparison was performed using two-sided log-rank test. ****$P = 3.8 \times 10^{-8}$. **d**,**e**, Hallmark gene set enrichment analysis of **d**, patients with mRD ($n = 19$) versus with mCR after surgery ($n = 7$), and **e**, patients with mRD ($n = 11$) versus with mCR after BCG ($n = 8$). **f**, Heatmap of urine cfRNA gene expression for previously defined immune and proliferation-related gene signatures in patients with mRD ($n = 11$) and mCR ($n = 8$) after BCG. **g**, T cell receptor clones per million reads in urine cfRNA from patients with mRD ($n = 10$) versus with mCR ($n = 7$) after BCG. Comparison was performed using two-sided Mann–Whitney *U* test. *$P = 0.01$. **h**, T cell receptor diversity in urine cfRNA from patients with mRD ($n = 10$) versus with mCR ($n = 7$) after BCG calculated using inverse Simpson index. Comparison was performed using two-sided Mann–Whitney *U* test. *$P = 0.04$. In box plots, the center line denotes the median, the box contains the IQR, and the whiskers extend to 1.5× IQR. mem, memory; MHC, major histocompatibility complex; STING, stimulator of interferon genes; TCR, T cell receptor; UV, ultraviolet; ND, not detected; Act., activated. Panel **a** created in BioRender; Shi, W. https://biorender.com/wc0ub9j (2026).

We observed that the specificity of urine cfRNA-based BLCA detection does not appear to be affected by the presence of field-effect mutations. We hypothesize that this is because expression programs of urothelial cells containing field-effect mutations are more similar to those of normal urothelial cells than BLCA cells. Our detection model was also able to identify molecular evidence of residual disease following surgery and adjuvant therapy with high sensitivity and specificity, supporting a role for urine cfRNA analysis in MRD assessment. While these results are encouraging, larger cohorts and prospective clinical trials will be required to define fully the performance characteristics and clinical utility of cfRNA analysis in these settings.

A key distinguishing feature of cfRNA compared to utDNA approaches is the ability to profile the expression of thousands of genes, enabling characterization of tumor biology. We demonstrated the ability to distinguish clinically relevant BLCA subgroups, such as LG versus HG NMIBC and NMIBC versus MIBC. Among tumors classified as LG by histopathology, higher cfRNA grade scores were associated with increased risk of recurrence, suggesting cfRNA can detect features not

https://doi.org/10.1038/s41591-026-04673-3

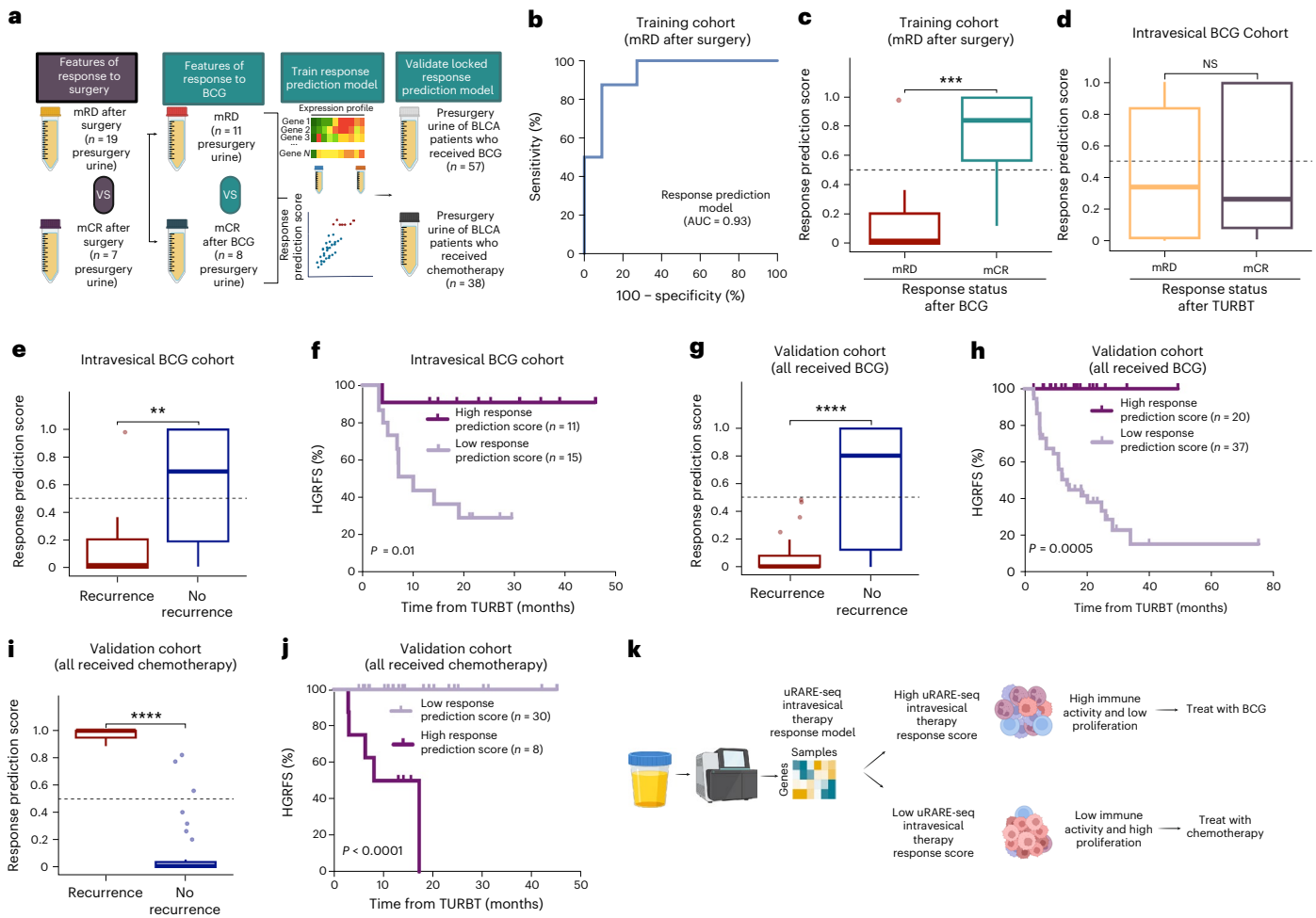


Fig. 6 | Predicting response to intravesical therapy using uRARE-seq. a, Schematic for training and validating the intravesical therapy response prediction model. **b**, ROC analysis of uRARE-seq response prediction model in the BCG training cohort. **c**, Response prediction scores from patients with no mCR ($n = 11$) versus with mCR after BCG ($n = 8$). Comparison was performed using two-sided Mann–Whitney U test. Dashed line indicates response prediction score cutoff and was selected based on optimal performance in the training cohort using the Survminer R package. ***$P = 0.0007$. **d**, The same as in **c** but from patients with mRD ($n = 19$) versus with mCR after surgery ($n = 7$). **e**, Response prediction scores stratified by clinical recurrence ($n = 11$) versus no recurrence ($n = 15$). Dashed line indicates the response prediction score cutoff. Comparisons were performed using two-sided Mann–Whitney U test. **$P = 0.003$. **f**, Kaplan–Meier analysis using presurgery urine samples stratified by high (above cutoff) versus low (below cutoff) response prediction scores. Comparison was performed using two-sided log-rank test. **g**, Response prediction scores in the BCG validation cohort stratified by clinical recurrence ($n = 26$) versus no recurrence ($n = 31$). Dashed line indicates the response prediction score threshold locked in the training cohort. Comparison was performed using two-sided Mann–Whitney U test. ****$P = 2.3 \times 10^{-7}$. **h**, Kaplan–Meier analysis using presurgery urine samples from the BCG validation cohort stratified by high (above cutoff) versus low (below cutoff) response prediction scores. Comparison was performed using the two-sided log-rank test. **i**, Response prediction scores in the intravesical chemotherapy validation cohort stratified by clinical recurrence ($n = 5$) versus no recurrence ($n = 33$). Dashed line indicates the response prediction score threshold locked in the training cohort. Comparison was performed using two-sided Mann–Whitney U test. ****$P = 3.9 \times 10^{-6}$. **j**, Kaplan–Meier analysis using presurgery urine samples from the intravesical chemotherapy cohort stratified by high (above cutoff) versus low (below cutoff) response prediction scores. Comparison was performed using the two-sided log-rank test. ****$P = 1.6 \times 10^{-5}$. **k**, Schematic of potential application of uRARE-seq for personalizing choice of intravesical adjuvant therapy in NMIBC. In box plots, the center line denotes the median, the box contains the IQR and the whiskers extend to 1.5× IQR. Panels created in BioRender: **a**, Shi, W. https://biorender.com/y4yqizc (2026); **k**, Shi, W. https://biorender.com/66ls98x (2026).

captured by microscopic evaluation. Analysis of cfRNA may therefore be useful for identifying LG patients who might benefit from more aggressive treatment regimens used for clinically high-risk patients[1]. Similarly, one potential use of the invasion model could be to identify patients with NMIBC who are at risk for having unrecognized MIBC and might have been understaged.

A key challenge in developing robust biomarkers of BCG response in NMIBC has been the inability to distinguish patients cured by surgery versus adjuvant BCG immunotherapy. Thus, although several biomarkers associated with long-term recurrence-free survival after surgery plus BCG have been proposed, these have been challenging to validate and none are used in routine clinical practice[30,46,49–55]. Since urine cfRNA analysis can identify patients who have complete molecular responses after surgery versus adjuvant treatment, we were able to identify biomarkers specific to BCG responders. Tumors from patients with clearance of BLCA cfRNA after BCG displayed higher expression of T cell and immune-related signatures and lower expression of proliferation-associated programs, suggesting an immune response needs to be present for BCG to be effective. Additionally, some of the enriched immune-related signatures are also overexpressed in advanced BLCA and other cancers that are more likely to respond to systemic immune checkpoint inhibitors[33,37], suggesting potential mechanistic similarities between these distinct immunotherapies.

The observation that tumors in patients with mRD after BCG expressed high levels of proliferation-associated genes led us to postulate that these patients might be more likely to respond to intravesical chemotherapy. Supporting this premise, a machine learning model integrating both immune- and proliferation-associated genes predicted the likelihood of responding to the two therapies. Our observation that patients unlikely to respond to BCG are more likely to respond to chemotherapy is consistent with clinical observations that patients with recurrence after BCG are more likely to respond to chemotherapy than repeat BCG[56] and that chemotherapy can achieve durable responses after BCG failure[57]. It will be interesting to compare and potentially integrate urine cfRNA analysis with other approaches for response prediction, such as digital pathology[58].

Currently, BCG is the preferred choice for first-line intravesical therapy. However, BCG availability is frequently limited by recurring supply shortages[59]. Therefore, a predictive biomarker to select patients who would benefit from first-line chemotherapy instead of BCG could be impactful. Before cfRNA-based treatment selection can be used clinically, additional studies will be needed to establish the clinical utility of such an approach.

Limitations of this study include its case–control design and that subjects were enrolled at two affiliated and geographically adjacent institutions. Validation in independent samples collected at the same sites confirmed robust performance, but sample sizes in some analyses were modest and potential unmeasured technical and clinical confounders cannot be excluded. While specificity remained high in the patients with nonmalignant GU conditions, the number of patients with each diagnosis was modest and not all potentially confounding clinical problems could be explored. Although the locked intravesical therapy response prediction model was validated in independent samples, these cohorts were not randomized, and treatment assignment could therefore have been influenced by unmeasured confounders. Therefore, larger prospective follow-up studies will be required to confirm the assay's technical performance characteristics and to establish its clinical utility for different applications.

In summary, urine cfRNA analysis using uRARE-seq enables sensitive detection and molecular characterization of BLCA, potentially enabling applications such as screening, MRD detection and adjuvant therapy response prediction. We envision that urine cfRNA analysis may also allow development of biomarkers for precision medicine applications in other malignant and benign GU diseases.

Online content

Any methods, additional references, Nature Portfolio reporting summaries, source data, extended data, supplementary information, acknowledgements, peer review information; details of author contributions and competing interests; and statements of data and code availability are available at https://doi.org/10.1038/s41591-026-04673-3.

References

1. Dyrskjøt, L. et al. Bladder cancer. *Nat. Rev. Dis. Primers* **9**, 1–21 (2023).
2. Flores Monar, G. V., Reynolds, T., Gordon, M., Moon, D. & Moon, C. Molecular markers for bladder cancer screening: an insight into bladder cancer and FDA-approved biomarkers. *Int. J. Mol. Sci.* **24**, 14374 (2023).
3. Sugeeta, S. S., Sharma, A., Ng, K., Nayak, A. & Vasdev, N. Biomarkers in bladder cancer surveillance. *Front. Surg.* **8**, 735868 (2021).
4. Shkolyar, E. et al. Bladder cancer risk stratification using a urinary mRNA biomarker panel—a path towards cystoscopy triaging. *Urol. Oncol.* **39**, 497.e9–497.e15 (2021).
5. Chou, R. et al. Urinary biomarkers for diagnosis of bladder cancer: a systematic review and meta-analysis. *Ann. Intern. Med.* **163**, 922–931 (2015).
6. Lin, S. Y., Linehan, J. A., Wilson, T. G. & Hoon, D. S. B. Emerging utility of urinary cell-free nucleic acid biomarkers for prostate, bladder, and renal cancers. *Eur. Urol. Focus* **3**, 265–272 (2017).
7. Hong, M. et al. Biomarkers for precision urothelial carcinoma diagnosis: current approaches and the application of single-cell technologies. *Cancers* **13**, 260 (2021).
8. Nesselbush, M. C. et al. An ultrasensitive method for detection of cell-free RNA. *Nature* **4**, 1–10 (2025).
9. Valenberg, F. J. P. et al. Prospective validation of an mRNA-based urine test for surveillance of patients with bladder cancer. *Eur. Urol.* **75**, 853–860 (2019).
10. Salomo, K. et al. Urinary transcript quantitation of CK20 and IGF2 for the non-invasive bladder cancer detection. *J. Cancer Res. Clin. Oncol.* **143**, 1757–1769 (2017).
11. Rasti, A. et al. Evaluation of IGF2, KRT14, and KRT20 as urinary biomarkers in patients with bladder cancer. *Rep. Biochem. Mol. Biol.* **11**, 710 (2023).
12. Volkmer, J. P. et al. Three differentiation states risk-stratify bladder cancer into distinct subtypes. *Proc. Natl Acad. Sci. USA* **109**, 2078–2083 (2012).
13. Papafotiou, G. et al. KRT14 marks a subpopulation of bladder basal cells with pivotal role in regeneration and tumorigenesis. *Nat. Commun.* **7**, 11914 (2016).
14. Kang, W. et al. The SLC family are candidate diagnostic and prognostic biomarkers in clear cell renal cell carcinoma. *Biomed Res. Int.* **2020**, 1025178 (2020).
15. Simon, A. G. et al. RNA sequencing reveals alterations and similarities in cell metabolism, hypoxia and immune evasion in primary cell cultures of clear cell renal cell carcinoma. *Front. Oncol.* **12**, 883195 (2022).
16. You, Y., Ren, Y., Liu, J. & Qu, J. Promising epigenetic biomarkers associated with cancer-associated-fibroblasts for progression of kidney renal clear cell carcinoma. *Front. Genet.* **12**, 736156 (2021).
17. Alchahin, A. M. et al. A transcriptional metastatic signature predicts survival in clear cell renal cell carcinoma. *Nat. Commun.* **13**, 5747 (2022).
18. Tan, M. H. E., Li, J., Xu, H. E., Melcher, K. & Yong, E.-l. Androgen receptor: structure, role in prostate cancer and drug discovery. *Acta Pharmacol. Sin.* **36**, 3–23 (2015).
19. Thorek, D. L. J., Evans, M. J., Carlsson, S. V., Ulmert, D. & Lilja, H. Prostate-specific kallikrein-related peptidases and their relation to prostate cancer biology and detection. Established relevance and emerging roles. *Thromb. Haemost.* **110**, 484–492 (2013).
20. Cao, Z. et al. Overexpression of transglutaminase 4 and prostate cancer progression: a potential predictor of less favourable outcomes. *Asian J. Androl.* **15**, 742–746 (2013).
21. Fernández, C. A. et al. A novel approach to using matrix metalloproteinases for bladder cancer. *J. Urol.* **182**, 2188–2194 (2009).
22. Rodriguez Faba, O. et al. Matrix metalloproteinases and bladder cancer: what is new? *ISRN Urol.* **2012**, 581539 (2012).
23. Lotan, Y. & Roehrborn, C. G. Sensitivity and specificity of commonly available bladder tumor markers versus cytology: results of a comprehensive literature review and meta-analyses. *Urology* **61**, 109–118 (2003).
24. Zhang, M. L. et al. A review of urinary cytology in the setting of upper tract urothelial carcinoma. *J. Am. Soc. Cytopathol.* **10**, 29–35 (2021).
25. Messer, J. et al. Urinary cytology has a poor performance for predicting invasive or high-grade upper-tract urothelial carcinoma. *BJU Int.* **108**, 701–705 (2011).
26. Dudley, J. C. et al. Detection and surveillance of bladder cancer using urine tumor DNA. *Cancer Discov.* **9**, 500–509 (2019).
27. Shi, W. Y. et al. Field-effect-informed urine liquid biopsy for bladder cancer. *Cell* **189**, 1024–1038.e9 (2026).

28. D'Elia, C. et al. Diagnostic value of Xpert® Bladder Cancer Monitor in the follow-up of patients affected by non-muscle invasive bladder cancer: an update. *Ther. Adv. Urol.* **13**, 1756287221997183 (2021).
29. Gopalakrishna, A. et al. Anticipatory positive urine tests for bladder cancer. *Ann. Surg. Oncol.* **24**, 1747–1753 (2017).
30. Lindskrog, S. V. et al. An integrated multi-omics analysis identifies prognostic molecular subtypes of non-muscle-invasive bladder cancer. *Nat. Commun.* **12**, 1–18 (2021).
31. Sjödahl, G., Bernardo, C., Eriksson, P., Höglund, M. & Liedberg, F. Tumor biomarkers for Bacillus Calmette-Guérin response: what we get is not what we want. *Eur. Urol. Focus* **9**, 582–583 (2023).
32. Wang, Z. et al. Predictive biomarkers of response to Bacillus Calmette-Guérin immunotherapy and Bacillus Calmette-Guérin failure for non-muscle invasive bladder cancer. *Int. J. Urol.* **29**, 807–815 (2022).
33. Ayers, M. et al. IFN-γ-related mRNA profile predicts clinical response to PD-1 blockade. *J. Clin. Invest.* **127**, 2930–2940 (2017).
34. Oh, D. Y. et al. Intratumoral CD4+ T cells mediate anti-tumor cytotoxicity in human bladder cancer. *Cell* **181**, 1612–1625.e13 (2020).
35. Mariathasan, S. et al. TGFβ attenuates tumour response to PD-L1 blockade by contributing to exclusion of T cells. *Nature* **554**, 544–548 (2018).
36. Jerby-Arnon, L. et al. A cancer cell program promotes T cell exclusion and resistance to checkpoint blockade. *Cell* **175**, 984–997.e24 (2018).
37. Rijnders, M. et al. Gene-expression-based T-Cell-to-Stroma Enrichment (TSE) score predicts response to immune checkpoint inhibitors in urothelial cancer. *Nat. Commun.* **15**, 1–13 (2024).
38. Lowery, F. J. et al. Molecular signatures of antitumor neoantigen-reactive T cells from metastatic human cancers. *Science* **375**, 877–884 (2022).
39. Zheng, L. et al. Pan-cancer single-cell landscape of tumor-infiltrating T cells. *Science* **374**, abe6474 (2021).
40. Rooney, M. S., Shukla, S. A., Wu, C. J., Getz, G. & Hacohen, N. Molecular and genetic properties of tumors associated with local immune cytolytic activity. *Cell* **160**, 48–61 (2015).
41. Mami-Chouaib, F. et al. Resident memory T cells, critical components in tumor immunology. *J. Immunother. Cancer* **6**, 87 (2018).
42. Milner, J. J. & Goldrath, A. W. Transcriptional programming of tissue-resident memory CD8+ T cells. *Curr. Opin. Immunol.* **51**, 162–169 (2018).
43. Sautès-Fridman, C., Petitprez, F., Calderaro, J. & Fridman, W. H. Tertiary lymphoid structures in the era of cancer immunotherapy. *Nat. Rev. Cancer* **19**, 307–325 (2019).
44. Choo, S. Y. The HLA system: genetics, immunology, clinical testing, and clinical implications. *Yonsei Med. J.* **48**, 11 (2007).
45. Thompson, J. C. et al. Gene signature of antigen processing and presentation machinery predicts response to checkpoint blockade in non-small cell lung cancer (NSCLC) and melanoma. *J. Immunother. Cancer* **8**, e000974 (2020).
46. de Jong, F. C. et al. Non–muscle-invasive bladder cancer molecular subtypes predict differential response to intravesical Bacillus Calmette-Guérin. *Sci. Transl. Med.* **15**, eabn4118 (2023).
47. Kurtz, D. M. et al. Enhanced detection of minimal residual disease by targeted sequencing of phased variants in circulating tumor DNA. *Nat. Biotechnol.* **39**, 1537–1547 (2021).
48. Cohen, J. D. et al. Detection of low-frequency DNA variants by targeted sequencing of the Watson and Crick strands. *Nat. Biotechnol.* **39**, 1220–1227 (2021).
49. Kjær, A. et al. Low T cell diversity associates with poor outcome in bladder cancer: a comprehensive longitudinal analysis of the T cell receptor repertoire. *Cell Rep. Med.* **6**, 102101 (2025).
50. Bellmunt, J. et al. Genomic predictors of good outcome, recurrence, or progression in high-grade T1 non-muscle-invasive bladder cancer. *Cancer Res.* **80**, 4476–4486 (2020).
51. Bacon, J. V. W. et al. Somatic features of response and relapse in non-muscle-invasive bladder cancer treated with Bacillus Calmette-Guérin immunotherapy. *Eur. Urol. Oncol.* **5**, 677–686 (2022).
52. Batista, R. et al. TERT promoter mutation as a potential predictive biomarker in BCG-treated bladder cancer patients. *Int. J. Mol. Sci.* **21**, 947 (2020).
53. Pietzak, E. J. et al. Next-generation sequencing of nonmuscle invasive bladder cancer reveals potential biomarkers and rational therapeutic targets. *Eur. Urol.* **72**, 952–959 (2017).
54. Strandgaard, T. et al. Elevated T-cell exhaustion and urinary tumor DNA levels are associated with Bacillus Calmette-Guérin failure in patients with non-muscle-invasive bladder cancer. *Eur. Urol.* **82**, 646–656 (2022).
55. Roumiguié, M. et al. PD-L1 expression and pattern of immune cells in pre-treatment specimens are associated with disease-free survival for HR-NMIBC undergoing BCG treatment. *World J. Urol.* **39**, 4055–4065 (2021).
56. Taylor, J. et al. Oncologic outcomes of sequential intravesical gemcitabine and docetaxel compared with Bacillus Calmette-Guérin in patients with Bacillus Calmette-Guérin-unresponsive non-muscle invasive bladder cancer. *Eur. Urol. Oncol.* **8**, 469–476 (2025).
57. Steinberg, R. L. et al. Multi-Institution evaluation of sequential gemcitabine and docetaxel as rescue therapy for nonmuscle invasive bladder cancer. *J. Urol.* **203**, 902–908 (2020).
58. Packiam, V. T. et al. Presence of an artificial intelligence-powered predictive biomarker is associated with a poor response to intravesical Bacillus Calmette-Guerin but not to intravesical sequential gemcitabine/docetaxel in patients with high-grade non-muscle-invasive bladder cancer. *Eur. Urol. Oncol.* **8**, 1461–1465 (2025).
59. Lobo, N. et al. 100 years of Bacillus Calmette–Guérin immunotherapy: from cattle to COVID-19. *Nat. Rev. Urol.* **18**, 611–622 (2021).
60. Newman, A. M. et al. Determining cell type abundance and expression from bulk tissues with digital cytometry. *Nat. Biotechnol.* **37**, 773–782 (2019).

Publisher's note Springer Nature remains neutral with regard to jurisdictional claims in published maps and institutional affiliations.

Open Access This article is licensed under a Creative Commons Attribution-NonCommercial-NoDerivatives 4.0 International License, which permits any non-commercial use, sharing, distribution and reproduction in any medium or format, as long as you give appropriate credit to the original author(s) and the source, provide a link to the Creative Commons licence, and indicate if you modified the licensed material. You do not have permission under this licence to share adapted material derived from this article or parts of it. The images or other third party material in this article are included in the article's Creative Commons licence, unless indicated otherwise in a credit line to the material. If material is not included in the article's Creative Commons licence and your intended use is not permitted by statutory regulation or exceeds the permitted use, you will need to obtain permission directly from the copyright holder. To view a copy of this licence, visit http://creativecommons.org/licenses/by-nc-nd/4.0/.

© The Author(s) 2026

https://doi.org/10.1038/s41591-026-04673-3

Kevin J. Liu[1,2,3], William Y. Shi[1,2,3], Monica C. Nesselbush[4], Nick A. Phillips[1,3,5], Kathleen E. Mach[6,7], Bogdan Luca[8], Ravi K. Bajpai[1,2], Isabel Jabara[1,2], Jordan C. Cheng[1,2], Takeshi Sugio[1,5], Navika Shukla[1,5], Emily C. Shen[1,2,3], Ivy Lee Koh[1,2], Douglas J. Wu[8], Chih-Long Liu[1,5], Diego Almanza[1,2,3], Soyeong Jun[1,2], Feng Tian[1,2,5], Emily G. Hamilton[4], Christian R. Hoerner[1,9,10], Rui Wang[1,2,5], Mohammad S. Esfahani[1,2], Angela Hui[1,2], Vinh La[6,7], Grace Holton[6,7], Gabriela Rodriguez[6,7], Timothy J. Lee[6,7], Xi Ling[2], Nikitha Kalahasti[2], Spoorthi Vallamkonda[2], Patrick Mullane[8], Simon B. Chen[8], Eugene Shkolyar[6], Kris Prado[6], Ali Raza Khaki[10], Emily Chan[8], Mark K. Buyyounouski[2], Alice C. Fan[1,5,9,10], Eila C. Skinner[6], Ash A. Alizadeh[1,5,10,11] ✉, Joseph C. Liao[1,6,7] ✉ & Maximilian Diehn[1,2,11] ✉

[1]Stanford Cancer Institute, Stanford University, Stanford, CA, USA. [2]Department of Radiation Oncology, Stanford University, Stanford, CA, USA. [3]Program in Cancer Biology, Stanford University, Stanford, CA, USA. [4]Resero Bio, San Carlos, CA, USA. [5]Division of Oncology, Department of Medicine, Stanford University, Stanford, CA, USA. [6]Department of Urology, Stanford University, Stanford, CA, USA. [7]Veterans Affairs Palo Alto Health Care System, Palo Alto, CA, USA. [8]Department of Pathology, Stanford University, Stanford, CA, USA. [9]Canary Center at the Stanford School of Medicine, Stanford University, Stanford, CA, USA. [10]Division of Hematology, Department of Medicine, Stanford University, Stanford, CA, USA. [11]Institute for Stem Cell Biology and Regenerative Medicine, Stanford University, Stanford, CA, USA. ✉e-mail: arasha@stanford.edu; jliao@stanford.edu; diehn@stanford.edu

Methods

Human participants and cohorts

All samples analyzed in this study were collected using protocols approved by Institutional Review Boards (IRBs) at their respective centers. Collection centers included Stanford University and Stanford Health Care and the Veterans Affairs Palo Alto Health Care System (VA Palo Alto). BLCA cases were collected under IRB 55427. The control cases were collected under IRB 55427, 12597 or 18225. RCC samples were collected under IRB 12597. Prostate cancer samples were collected under IRB 49693. All participants provided written informed consent for use of their clinical data and biospecimens for research. In total, 683 urine samples were collected from 515 individuals. The clinical and demographic characteristics such as age, sex and smoking history of participants are presented in Supplementary Table 1 and consent was obtained to publish clinical and demographic characteristics. Sex and smoking history were self-reported and identified from medical records. Participants were not compensated for their participation in this study. Risk stratification was performed using the American Urological Association risk classification system, which is based on factors such as tumor grade, stage, size and the presence of carcinoma in situ[61].

Cancer cohorts. Patients with BLCA, PRAD or kidney cancer enrolled at Stanford University or VA Palo Alto.

Noncancer cohorts. Individuals who were either asymptomatic, had hematuria or had lower urinary tract symptoms such as frequent urination, difficulty with urination or discomfort during urination enrolled at Stanford University or VA Palo Alto.

Validation cohorts. Patients with BLCA and controls without cancer enrolled at Stanford University or VA Palo Alto but not used for model training.

Formalin-fixed paraffin-embedded tumor extraction, quantification and library prep

For comparison of BLCA tumor RNA versus urine cfRNA and the UROMOL/BRS subtype analyses, hematoxylin and eosin-stained sections from formalin-fixed paraffin-embedded (FFPE) bladder tumor blocks were annotated by a pathologist to identify regions containing tumor. BLCA grade and stage for each patient with BLCA were obtained from clinical pathology reports and notes. Core punches were performed on FFPE blocks targeting regions containing tumor tissue and RNA was extracted using CELLDATA DNAstorm/RNAstorm 2.0 Combination Kit (Biotium) according to the manufacturer's recommendation with minor modifications. The resulting eluate was incubated with 28 U DNase I (RNase-Free DNase Set, Qiagen) for 30 minutes at room temperature to remove DNA. RNA was subsequently isolated using the Zymo RNA Clean & Concentrator kit and stored at −80 °C. Concentration of RNA was quantified using Nanodrop or quantitative PCR (qPCR). For library preparation, 100 ng of RNA was input into library preparation. For samples with less than 100 ng of RNA, all extracted tumor RNA was used for library preparation (range 25–100 ng). Double-stranded complementary DNA (cDNA) was synthesized from tumor RNA using the NEBNext Ultra™ II RNA First-Strand Synthesis Module and Non-Directional Second Strand Synthesis Module (New England Biolabs). Double-stranded cDNA was treated with 100 U S1 nuclease (Thermo Fisher) for 30 minutes at room temperature to hydrolyze single-stranded regions. The KAPA Hyper Prep kit (Kapa Biosystems) was used to prepare libraries for sequencing, following the manufacturer's instructions with slight modifications, as previously described[62]. Whole-coding transcriptome capture was performed using the Twist Biosciences Comprehensive Exome Hybridization kit, following respective manufacturer's instructions. Captured libraries were sequenced using 2 × 150 bp paired-end reads on Illumina HiSeq4000 or NovaSeq6000 instruments. For tumor FFPE samples captured using the whole-coding transcriptome capture panel, we targeted ~30 million read pairs.

Urine collection and processing

First void urine samples were collected before any instrumentation into empty 120 ml urine collection cups (with or without subsequent addition of ethylenediaminetetraacetic acid to a final concentration of 5 mM) or Norgen Urine Collection and Stabilization Cups. Within 24 hours, urine supernatant was isolated using centrifugation at 2000*g* for 10 minutes. Urine supernatant was stored at −80 °C until cell-free nucleic acid isolation.

cfRNA extraction and DNA digestion

Q-Sepharose resin-based method. Cell-free nucleic acids were extracted from urine using a previously published protocol[26] optimized for urine cfDNA extraction. The resulting eluate was incubated with 14 U DNase I (RNase-Free DNase Set, Qiagen) for 30 minutes at room temperature to digest DNA. The digested eluate was purified using the Zymo RNA Clean & Concentrator kit and stored at −80 °C.

Standard QIAamp method. Cell-free nucleic acids were extracted from urine using a previously published protocol[62]. The resulting eluate was incubated with 14 U DNase I (RNase-Free DNase Set, Qiagen) for 30 minutes at room temperature to digest DNA. RNA was purified using the Zymo RNA Clean & Concentrator kit and stored at −80 °C.

Modified QIAamp method. Cell-free nucleic acids were extracted from urine using the miRNA protocol from the QIAamp Circulating Nucleic Acid kit (Qiagen (range 1–20 ml)) with slight modification. The modifications include scaling reagents proportionally to accommodate >4 ml of urine, increasing lysis incubation time from 30 minutes to 60 minutes, and performing a double elution of the column to maximize RNA yield. The resulting eluate was incubated with 14 U DNase I (RNase-Free DNase Set, Qiagen) for 30 minutes at room temperature to digest DNA. The digested eluate was purified using the Zymo RNA Clean & Concentrator kit and stored at −80 °C.

cfRNA size evaluation and quantification

The urine cfRNA size distribution was analyzed using Agilent Bioanalyzer RNA 6000 Pico chip. Quantitative real-time polymerase chain reaction was used for quantification of cfRNA. An RNA-targeted amplicon was designed and generated by Elim Biopharmaceuticals to span the boundary between exons 1 and 2 in the housekeeping gene POLR2A (Forward 5′-TGAGTCCGGATGAACTGAAGC-3′, Reverse 5′-CCCTCAGTCGTCTCTGGGTA-3′). A DNA-specific primer pair was designed to cover a 78 bp transcriptionally silent region of chromosome 12 (Forward 5′-TACGGTTGGTCCTTTCTTCG-3′, Reverse 5′-TTTCCTTTGGGTCTGAATGC-3′). Reverse transcription was first performed using the High-Capacity cDNA Reverse Transcription kit (Applied Biosystems). qPCR was then performed using 2X Power SYBR Green PCR Master Mix (Thermo Fisher Scientific) on Applied Biosystems 7500 Fast Real-Time PCR or QuantStudio 7 Pro instruments. Universal Human Reference RNA (Thermo Fisher Scientific) was run in parallel to generate a standard curve, and cfRNA concentrations were calculated by comparing the sample's POLR2A Ct value to the standard curve. If DNA was detected using the DNA-specific primer, DNA digestion, clean-up and quantification was repeated.

cfRNA library preparation and sequencing

uRARE-seq. We targeted an input mass of 500 pg cfRNA. For samples with less than 500 pg, all extracted cfRNA was used for library preparation (range 8–500 pg). Double-stranded cDNA was synthesized from cfRNA using the NEBNext Ultra™ II RNA First-Strand Synthesis Module and Non-Directional Second Strand Synthesis Module (New England

Biolabs). Double-stranded cDNA was treated with 100 U S1 nuclease (Thermo Fisher) for 30 minutes at room temperature to hydrolyze incomplete (single-stranded) regions. The KAPA Hyper Prep kit (Kapa Biosystems) was used to prepare libraries for sequencing, following the manufacturer's instructions with slight modifications, as previously described[62]. Whole-coding transcriptome capture was performed using the Twist Biosciences Comprehensive Exome Hybridization kit, following the manufacturer's instructions. Single-plex capture using the uRAG capture panel (see 'uRAG-focused capture panel design' for details) was performed using the Twist Biosciences Hybridization kit (Supplementary Table 3). Captured libraries were sequenced using 2 × 150 bp paired-end reads on Illumina HiSeq4000 or NovaSeq6000 instruments. For urine samples captured using the whole-coding transcriptome panel, we targeted ~30 million read pairs. For urine samples captured using the uRAG panel, we targeted 50–60 million read pairs.

Mapping, deduplication and quality control for uRARE-seq and tumor FFPE RNA

FASTQ files were demultiplexed using a custom pipeline, as previously described[62]. Fastp (v0.20.0) was used to trim the first 10 bases from the 5′ end of Read 1 and the 3′ end of Read 2 and to remove low-quality or short (< 35 bp) read pairs from each sample. Remaining high-quality reads were aligned to the reference transcriptome (GENCODE v27) and to the human genome (hg19) using STAR 2-pass[63] (v2.7.0). PCR duplicates were removed from both transcriptome-aligned and genome-aligned files using a custom barcoding approach. Deduplicated reads were used for gene-level expression estimation using RSEM (v1.2.28)[64].

Quality control was assessed using the RNASeQC package (v2.3.5), focusing on read mapping quality, mapping rates and rates of exonic, intronic, intergenic and ribosomal RNA reads. In addition, DNA contamination was estimated by calculating the percentage of reads that map to intronic sequences out of the total number of reads that map to exonic sequences.

Gene expression normalization

RSEM expected counts for captured genes were used for expression analyses (tximport R package v1.22). Counts were first normalized using the TMM method, which accounts for sample-to-sample variation in library size and transcriptome complexity (edgeR R package v3.36). Log-transformed and normalized expression values are referred to as '$\log_2$NX (normalized expression)'.

Differential gene expression analysis

Differential gene expression analysis was performed using DESeq2[65] (DESeq2 R package v1.34). GSEA was performed using the fgsea R package (v1.20). GSEA was performed using hallmark gene sets from MSigDB[66,67]. For GSEA, the hallmark pancreas beta cells and bile acid metabolism gene sets were excluded because these pathways have been shown to be nonspecific[68] and/or were not deemed relevant.

CIBERSORTx deconvolution

CIBERSORTx deconvolution was performed on normalized gene expression data using the previously published TM4 gene signature matrix[60].

Tissue and cell-type gene signatures

Tissue signatures were identified using gene expression data from the Genotype-Tissue Expression (GTEx)[69] project. Gene-level read counts generated by the UCSC Toil RNA sequencing bioinformatic pipeline were accessed in the UCSC Xena repository[70]. Gene expression was TMM-normalized. The normal tissue types that were evaluated from GTEx included bladder (n = 9), brain (n = 1,107), breast (n = 168), colon (n = 261), esophagus (n = 598), kidney (n = 24), liver (n = 97), lung (n = 241), ovary (n = 79), pancreas (n = 145), prostate (n = 86), skin (n = 497), stomach (n = 167) and whole blood (n = 290). Genes were defined as tissue-enriched if expression was 5-fold higher in each tissue compared to all other tissues and if average tissue $\log_2$NX was greater than zero.

For cell-type signatures, GU organs (kidney and bladder) and immune-related cell-type signatures were obtained from the PanglaoDB single-cell RNA sequencing database. Since prostate cells were not represented in PanglaoDB, prostate cell-type signatures were obtained from gene expression data downloaded from Tabula Sapiens[71]. Genes were defined as cell-type-enriched if their expression was 5-fold higher in the cell type compared to all cells in other major compartments (epithelial, endothelial, immune and stromal) and 2-fold higher in each cell subtype compared to cells within its own compartment.

For cancer-enriched genes, the cancer tissue types analyzed from the Cancer Genome Atlas (TCGA) included BLCA (n = 344), kidney (n = 350) and PRAD (n = 473). Cancer-enriched genes were defined as genes that are 5-fold higher in each cancer type compared to matched normal tissue expression data obtained from GTEx.

uRAG-focused capture panel design

To identify uRAGs, urine cfRNA gene expression data were analyzed from reference controls (n = 38) generated with the whole-coding transcriptome urine cfRNA-Seq method. Expression was TMM-normalized. RAGs were defined as genes that were expressed in less than 20% of samples and for which average $\log_2$NX was less than zero. In total, there were 3,834 uRAGs. RAGs are listed in Supplementary Table 2. Next, expression uniformity was calculated in cfRNA using the Gini coefficient, and endogenous control genes were selected from housekeeping genes[72] with a Gini <0.1. In addition, BLCA, PRAD and kidney cancer-associated genes from the literature were manually curated for inclusion in the panel, including genes that are recurrently mutated or rearranged in BLCA, PRAD and kidney cancer. In total, the RAG-focused capture panel consists of 4,782 unique genes (listed in Supplementary Table 3).

Generating machine learning models using elastic net

BLCA detection model. Elastic net logistic regression was used to train a urine cfRNA-based model to distinguish patients with BLCA (n = 151) from controls (n = 100). Nested 10-fold cross-validation was used to tune hyperparameters and estimate model performance (Sklearn Python package). Starting with all targeted genes, feature selection included:

(1) Removing genes that are differentially expressed between male and female reference controls (n = 38)
(2) Removing genes located on sex chromosomes
(3) Keeping genes that are differentially expressed between public BLCA RNA-Seq from TCGA (n = 407; downloaded from the UCSC Xena repository[70] and TMM-normalized) and reference control urine cfRNA (n = 38) using $P < 0.05$ and absolute $\log_2$ fold change of 3 as the cut point
(4) Removing genes with an average $\log_2$NX > 0 in GTEx blood samples and that are expressed in more than 20% of GTEx blood samples
(5) Removing immune-related genes included in the previously published CIBERSORTx LM22 gene list[60]
(6) Manually adding back '*TERT*' and '*IGF2*'

The list of genes (n = 381) and their coefficient values for the BLCA detection model is listed in Supplementary Table 4.

BLCA muscle invasion and BLCA grade models. For BLCA muscle invasion and BLCA grade models, only BLCA urine cfRNA samples that were detected in the BLCA detection model were considered for analysis. Elastic net logistic regression was used to train a urine cfRNA-based model to distinguish NMIBC (n = 116) from MIBC (n = 28)

and LG BLCA ($n = 31$) from HG BLCA ($n = 113$) urine samples. Nested 10-fold cross-validation was used to tune hyperparameters and estimate model performance (Sklearn Python packages). Starting with all targeted genes, feature selection included:

(1) Removing genes that are differentially expressed between male and female reference controls ($n = 38$)
(2) Removing genes located on sex chromosomes
(3) Keeping genes that are differentially expressed between:
  (a) For BLCA muscle invasion model: public NMIBC tumor RNA-Seq data from UROMOL ($n = 535$; downloaded from Lindskrog et al.[30] and TMM-normalized) and public MIBC RNA-Seq from TCGA ($n = 407$; downloaded from the UCSC Xena repository[70] and TMM-normalized) using $P < 0.05$ and absolute $\log_2$ fold change of 3 as the cut point
  (b) For BLCA grade model: differentially expressed genes between public LG BLCA and HG BLCA from UROMOL ($n = 535$; downloaded from Lindskrog et al.[30] and TMM-normalized)
(4) Removing genes with an average $\log_2$NX > 0 in GTEx blood samples and that are expressed in more than 20% of GTEx blood samples for BLCA grade model
(5) Removing immune-related genes included in the previously published CIBERSORTx LM22 gene list[60]
(6) Manually adding back '*KRT14*' for BLCA muscle invasion model

The list of genes (invasion model, 124; grade model, 294) and their coefficient values for the grade and muscle invasion classifier are listed in Supplementary Table 4.

Hypergeometric analysis of overlapping grade-associated genes in urine and tumor tissue

To determine the overlap between grade-associated genes in tumor tissue and urine, we first identified genes that were differentially expressed between LG and HG NMIBC tumors in the UROMOL cohort[30] and were included in the uRAG panel (log2 fold change > 1 and $P < 0.05$), yielding 57 LG-associated and 185 HG-associated tumor genes. We next identified genes differentially expressed in urine cfRNA from patients with LG versus HG NMIBC, yielding 158 LG-associated and 457 HG-associated urine genes. We then performed a hypergeometric test to assess the statistical significance of the observed overlap between tumor and urine gene sets, which comprised 33 LG-associated and 160 HG-associated genes. The total background gene set consisted of the 4,782 genes included in the uRAG panel.

Limit of detection estimation using BLCA tumor RNA spiked into urine cfRNA

To determine the LOD95 of uRARE-seq, we performed in silico spiking experiments using sequencing data from three healthy control urine samples and three BLCA tumor RNA samples generated using the uRAG-focused panel. Reads were randomly subsampled from these samples and combined in prespecified cancer fractions (range 0.001–50% allele frequency), determined based on the average somatic mutations' allele fraction identified using uCAPP-Seq[27] of the same BLCA RNA samples. The BLCA detection model described above was used to score each spiked-in sample for the uRAG capture panel. The limit of blank was calculated from the average and standard deviation of healthy cfRNA controls and was set as the detection threshold for remaining spikes. Logistic regression was employed to model the relationship between cancer spike-in fraction and BLCA detection, and LOD95 was defined as the cancer fraction where 95% of the spiked-in samples are detected.

Urine cytology

For urine cytology analysis, 'negative' or 'atypical' results were considered clinically negative and 'suspicious' or 'malignant' results were considered clinically positive[73].

Detection thresholds and classifying BCG molecular responses

The BLCA detection score thresholds for calling a sample positive were set based on specificity in noncancer controls in the training cohort. For modeling early detection applications using pretransurethral resection of bladder tumor samples, the threshold was set at 90% specificity (0.249). For MRD detection, the threshold was set at 99% specificity (0.83) for pre-BCG samples to account for potential expression changes due to recent surgery and 95% specificity (0.543) for post-BCG samples since they were months removed from surgery and BCG treatment.

Based on changes of BLCA detection scores, we defined BCG molecular response classes based on the following criteria:

(1) mCR after surgery: patients with BLCA detection score below the detection threshold after surgery (but before adjuvant therapy)
(2) mCR after BCG: patients with detectable BLCA detection score prior to BCG induction who, after completing BCG induction, have undetectable BLCA detection score
(3) mRD: patients with detectable BLCA detection score following BCG induction

utDNA analysis

For the comparisons between uRARE-seq and tumor-naive utDNA detection, mutation detection was performed using the tumor-naive uCAPP-Seq method from Dudley et al.[26]. For the comparison with tumor-informed utDNA detection, utDNA analysis was performed using RePhyNERX-enhanced uCAPP-Seq method (field-effect-informed) described in Shi et al.[27]. Briefly, the RePhyNERX removes likely field-effect mutations by analyzing the relative frequency of a somatic mutation in tumor tissue compared to all other mutations and compares this to its relative frequency in a urine sample. If the mutation is present at a higher relative frequency in a urine sample than expected, it is removed from consideration for MRD monitoring.

T cell clonality analysis

To facilitate T cell receptor analysis, the uRAG capture panel contains baits targeting the CDR3-proximal edges of the V genes and the junctions between the J and C genes. CDR3 sequences were analyzed using the SABER pipeline, as previously described[74].

Response prediction model signatures

Elastic net logistic regression was used to train a model to distinguish between no mCR and mCR to BCG using presurgery samples from the BCG training cohort. Leave-one-out cross-validation using the LeaveOneOut function (Sklearn) was used to evaluate the out-of-fold predictive performance of the model. For feature selection, in each leave-one-out cross-validation fold, differential gene expression (DESeq2) and gene set enrichment analysis (fgsea) were performed to identify pathway-informed leading-edge genes in the training fold cohort. Features considered for model training were limited to leading-edge genes from significant molecular signatures database pathways that are proliferation- and immune-related and genes identified from public literature, including:

- Interferon gamma response signatures[33]
- T cell signatures[33–37]

The R package Survminer was used to select the optimal cutoff (0.5) based on the BCG training cohort. The list of genes ($n = 623$) and their coefficients for the response prediction model classifier are listed in Supplementary Table 4.

Statistics and reproducibility

All statistical analyses were carried out using R v4.1.3 or Prism. Statistical tests used throughout the paper included Fisher's exact test,

Mann–Whitney *U* test, Student's t test, Pearson correlation and Friedman test. Kaplan–Meier curves were compared by the log-rank test, which was also used to derive hazard ratios. Unless *P* values are listed, significance labels used in the paper indicate: $*P < 0.05$; $**P < 0.01$; $***P < 0.001$ and $****P < 0.0001$. Unless otherwise specified, confidence intervals depict 95% confidence. No statistical method was used to predetermine sample size. No data were excluded from the analyses. The experiments were not randomized. The investigators were not blinded to allocation during experiments and outcome assessment.

Reporting summary

Further information on research design is available in the Nature Portfolio Reporting Summary linked to this article.

Data availability

Deidentified clinical and demographic data for individuals included in this study as well as model scores and other data are provided in the Supplementary Tables. Gene expression data from GTEx and TCGA were retrieved from the UCSC Xena Repository and derived from studies deposited in dbGaP (accession numbers phs000424 and phs000178, respectively). Gene expression data from the UROMOL BLCA study were obtained from Lindskrog et al.[30] (EGAS00001004693). Cell-type marker gene lists were downloaded from the PanglaoDB resource at https://panglaodb.se/markers.html. Custom gene signatures were generated using the Tabula Sapiens gene expression data[71]. Interferon gamma and T cell gene lists were obtained from Ayers et al.[33] and Rijnders et al.[37], respectively. The RNA sequencing data generated in this study are available in dbGaP (phs004116). Requests for additional information should be addressed to M.D.; requests will be addressed within 2 weeks.

Code availability

Code used in this study is available via GitHub at https://github.com/kevinjliustanford/uRARESeq.

References

61. Holzbeierlein, J. M. et al. Diagnosis and treatment of non-muscle invasive bladder cancer: AUA/SUO Guideline: 2024 Amendment. *J. Urol.* **211**, 533–538 (2024).
62. Chabon, J. J. et al. Integrating genomic features for non-invasive early lung cancer detection. *Nature* **580**, 245–251 (2020).
63. Dobin, A. et al. STAR: ultrafast universal RNA-seq aligner. *Bioinformatics* **29**, 15 (2013).
64. Li, B. & Dewey, C. N. RSEM: accurate transcript quantification from RNA-Seq data with or without a reference genome. *BMC Bioinformatics* **12**, 323 (2011).
65. Love, M. I., Huber, W. & Anders, S. Moderated estimation of fold change and dispersion for RNA-seq data with DESeq2. *Genome Biol.* **15**, 1–21 (2014).
66. Liberzon, A. et al. The Molecular Signatures Database (MSigDB) hallmark gene set collection. *Cell Syst.* **1**, 417–425 (2015).
67. Subramanian, A. et al. Gene set enrichment analysis: a knowledge-based approach for interpreting genome-wide expression profiles. *Proc. Natl Acad. Sci. USA* **102**, 15545–15550 (2005).
68. van Gurp, L. et al. Generation of human islet cell type-specific identity genesets. *Nat. Commun.* **13**, 2020 (2022).
69. Melé, M. et al. Human genomics. The human transcriptome across tissues and individuals. *Science* **348**, 660–665 (2015).
70. Goldman, M. J. et al. Visualizing and interpreting cancer genomics data via the Xena platform. *Nat. Biotechnol.* **38**, 675–678 (2020).
71. Jones, R. C. et al. The Tabula Sapiens: a multiple-organ, single-cell transcriptomic atlas of humans. *Science* **376**, eab14896 (2022).
72. Eisenberg, E. & Levanon, E. Y. Human housekeeping genes, revisited. *Trends Genet.* **29**, 569–574 (2013).
73. Brimo, F. et al. Accuracy of urine cytology and the significance of an atypical category. *Am. J. Clin. Pathol.* **132**, 785–793 (2009).
74. Sworder, B. J. et al. Determinants of resistance to engineered T cell therapies targeting CD19 in large B cell lymphomas. *Cancer Cell* **41**, 210–225.e5 (2023).

Acknowledgements

We would like to thank our patients for donating their time and samples for this study.

Author contributions

K.J.L., A.A.A., J.C.L. and M.D. developed the concept, designed the experiments and analyzed the data. K.J.L. and M.D. wrote the paper. K.J.L., M.C.N. and M.D. designed the experiments to identify uRAGs and developed the targeted selector used in this study. N.A.P. and B.L. developed the bioinformatic pipeline with input from K.J.L., W.Y.S., M.C.N., A.A.A. and M.D. Sample processing for clinical specimens was conducted by K.J.L., W.Y.S., K.E.M., R.K.B., J.C.C., C.R.H., V.L., G.H., G.R., T.J.L., A.H., X.L., N.K. and S.V. Bioinformatic analyses and interpretation were conducted by K.J.L., W.Y.S., M.C.N., N.A.P., B.L., I.J., E.C.S., T.S., N.S., D.A., S.J., E.G.H., R.W., M.S.E., A.A.A., J.C.L. and M.D. Software maintenance was performed by C.-L.L. and F.T. Patient specimens were collected and/or provided by K.E.M., C.R.H., V.L., G.H., G.R., T.J.L., X.L., N.K., S.V., E.S., K.P., A.R.K., M.K.B., A.C.F., E.C.S. and J.C.L. Pathology annotation was conducted by P.M., S.B.C., D.J.W. and E.C. Clinical data curation was performed by K.J.L., W.Y.S., K.E.M., C.R.H., A.C.F. and J.C.L. All authors reviewed the paper. The study was supervised by A.A.A., J.C.L. and M.D.

Funding

This work was supported by the Stanford ACED Canary Fellowship (K.J.L), Cui Scholar Graduate Fellowship (K.J.L), T32CA930245 (K.J.L.), the National Institutes of Health (R01CA244526 to A.A.A., J.C.L. and M.D.), NIH R01CA254179 (to M.D. and A.A.A.), K00 CA264398 (J.C.C.), Tobacco-Related Disease Research Program (TRDRP) (M.C.N. and W.Y.S.) and the Virginia and D.K. Ludwig Fund for Cancer Research and SDW/DT Philanthropic Gift (A.A.A. and M.D.).

Competing interests

K.J.L., W.Y.S., M.C.N. and E.G.H. report ownership interest or stock options in Resero Bio. M.S.E. and E.G.H. report consultancy for Foresight Diagnostics. M.C.N. and E.G.H. are employees of Resero Bio. A.A.A. has received research support from Celgene and Bristol Myers Squibb; reports consultancy for AstraZeneca, Arima, Natera, Roche, Genentech, Celgene, Bristol Myers Squibb, Forty Seven, Gilead, ADCT, Janssen, CARGO, Foresight Diagnostics, Adaptive Biotech and Chugai; has served on the Scientific Advisory Board for CiberMed and Foresight Diagnostics; and reports ownership interest in CiberMed, Resero Bio, Arima, Forty Seven, CARGO and Natera. J.C.L. reports consultancy for VPIX and UroViu and ownership interest or stock options in Resero Bio. M.D. reports current or past research support from AstraZeneca, Illumina and Varian; honoraria from Bristol Myers Squibb, Chugai and Novartis; consultancy to AstraZeneca, BioNTech, Boehringer Ingelheim, CiberMed, Foresight Diagnostics, Genentech, Gritstone Bio, Illumina, Natera, Perception Medicine, RefleXion, Regeneron, Resero Bio and Roche; patents licensed to Foresight Diagnostics, Natera, Resero Bio and Roche; and ownership interest or stock options in CiberMed, Foresight Diagnostics, Gritstone Bio, Natera, Perception Medicine and Resero Bio. K.J.L., W.Y.S., M.C.N., A.A.A., J.C.L. and M.D. also report patent filings related to urine cfRNA. The other authors declare no competing interests.

Additional information

Extended data is available for this paper at https://doi.org/10.1038/s41591-026-04673-3.

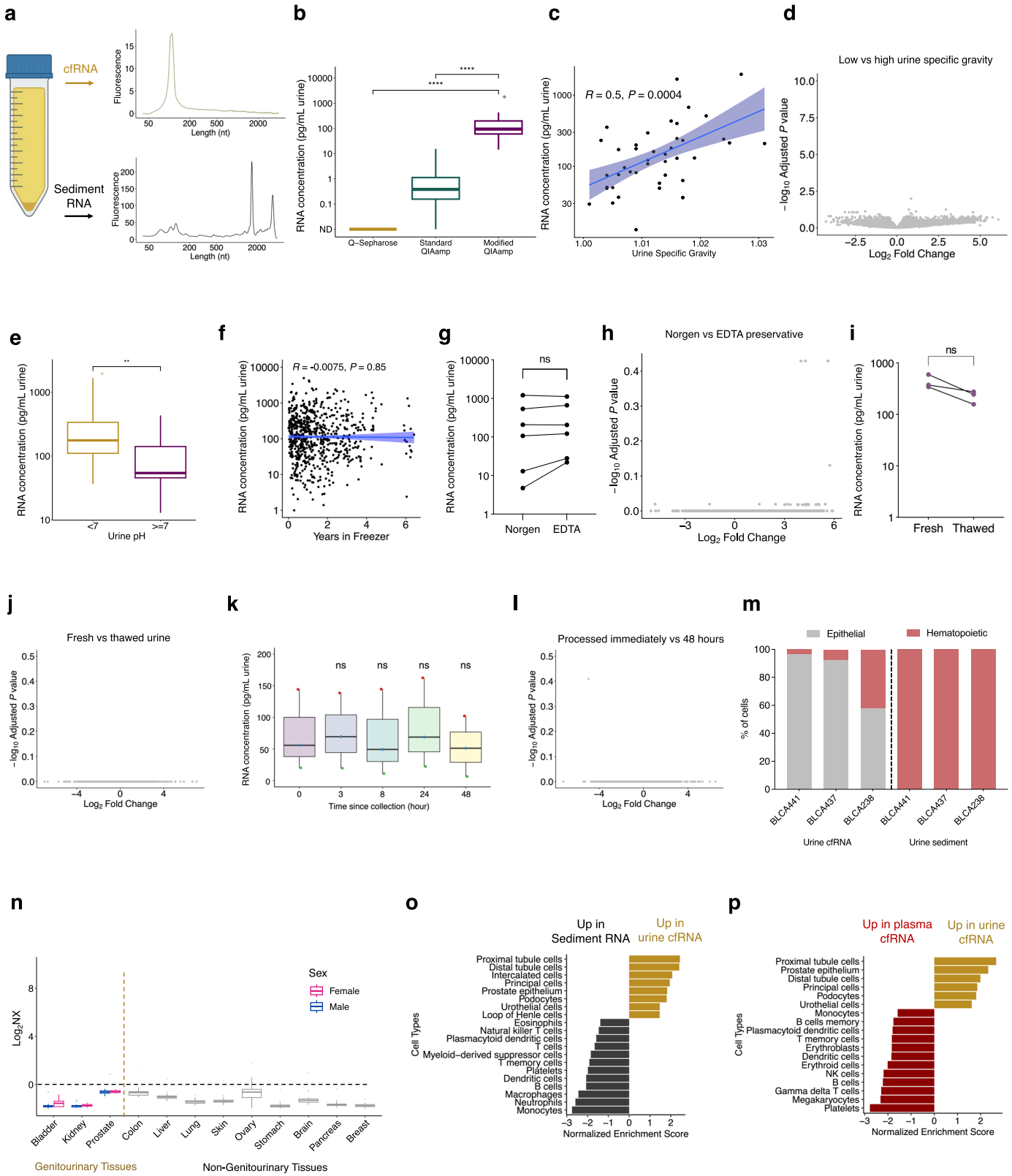
Supplementary information The online version contains supplementary material available at https://doi.org/10.1038/s41591-026-04673-3.

Correspondence and requests for materials should be addressed to Ash A. Alizadeh, Joseph C. Liao or Maximilian Diehn.

Peer review information *Nature Medicine* thanks David McConkey, Ana Vivancos and the other, anonymous, reviewer(s) for their contribution to the peer review of this work. Primary Handling Editor: Anna Ranzoni in collaboration with the *Nature Medicine* team.

Reprints and permissions information is available at www.nature.com/reprints.

https://doi.org/10.1038/s41591-026-04673-3

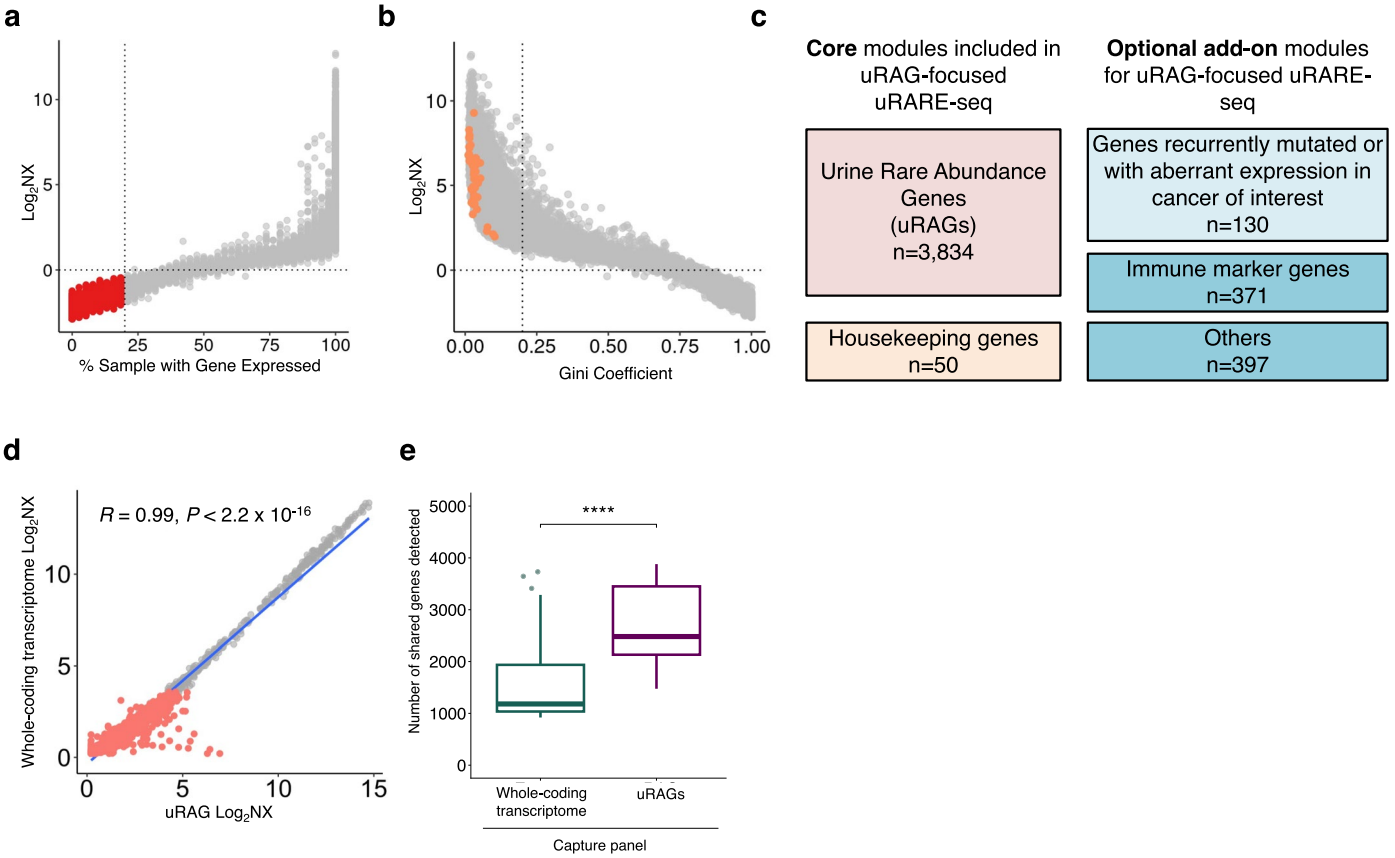


Extended Data Fig. 1 | See next page for caption.

https://doi.org/10.1038/s41591-026-04673-3

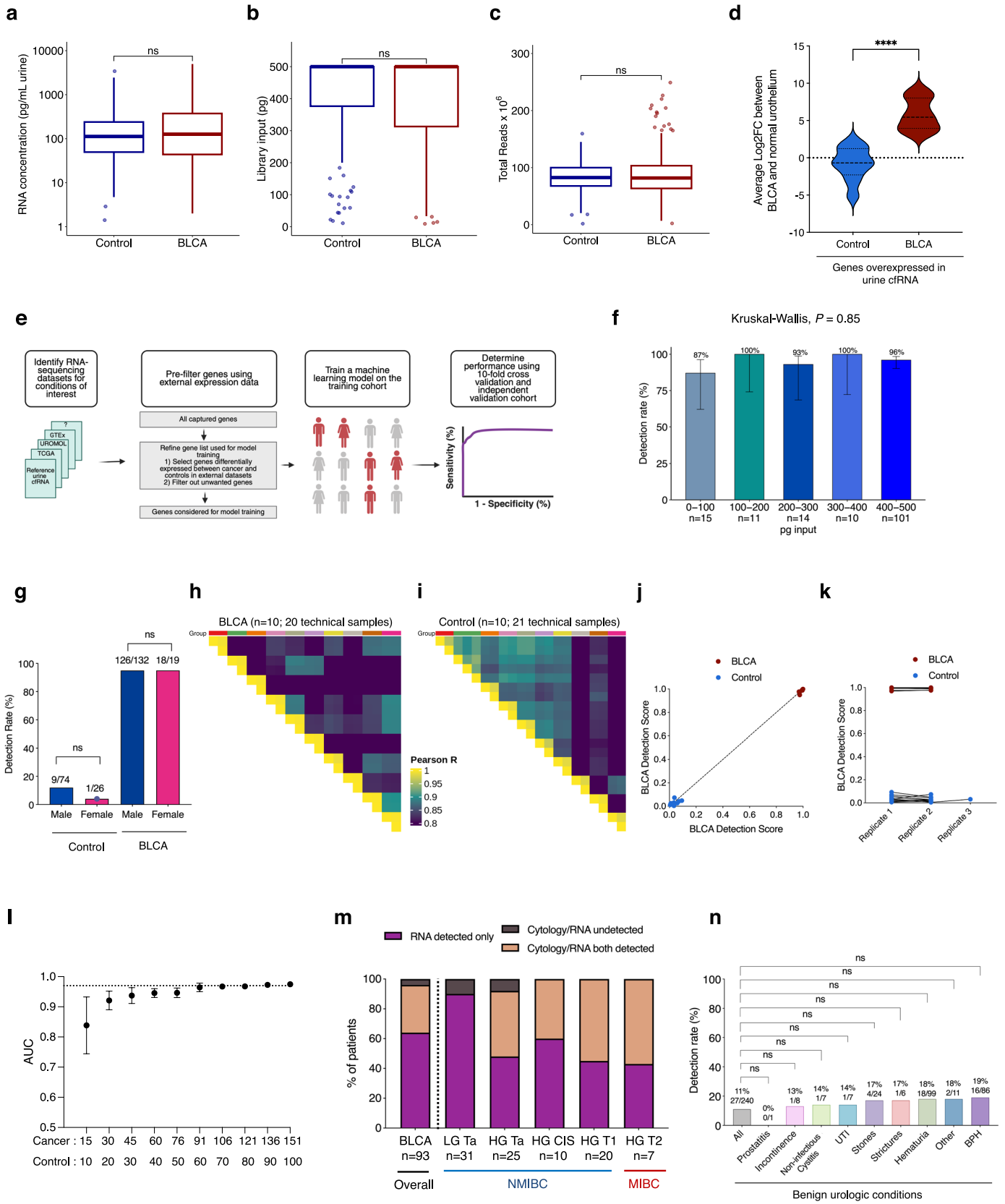
Extended Data Fig. 1 | Characterization of urine cfRNA. a, Representative bioanalyzer traces for urine cfRNA and urine sediment RNA. **b**, Urine cfRNA concentration (pg/mL of urine) extracted using Q-Sepharose ($n = 24$), standard QIAamp ($n = 33$), or modified QIAamp ($n = 48$) protocols measured using quantitative PCR. Statistical comparison was done using two-sided Student's t-test. ****$P \leq 2.2e\text{-}16$. **c**, Correlation between urine cfRNA concentration (pg/mL) and specific gravity ($n = 46$). Blue ribbon indicates 90% confidence interval. Pearson Correlation is shown. **d**, Volcano plot of differential gene expression comparing non-cancer controls (n=46) in the top and bottom quantiles of specific gravity. **e**, RNA concentration (pg/mL of urine) stratified by urine pH <7 ($n = 30$) and ≥7 ($n = 16$). Comparison was performed using two-sided Student's t-test. **$P = 0.002$. **f**, Association analysis between urine cfRNA concentration and sample storage time in −80C freezer ($n = 683$). Blue ribbon indicates 90% confidence interval. **g**, Comparison of urine cfRNA concentration (pg/mL) measured by qPCR using Norgen Collection and Stabilization Cup (Norgen Biotek) or EDTA ($n = 6$ paired samples) as preservative during urine collection. Comparison was performed using two-sided paired Student's t-test. **h**, Differential gene expression analysis between paired urine samples ($n = 6$) collected using Norgen Urine Collection and Stabilization Cup (Norgen Biotek) versus EDTA preservatives. **i**, Comparison of urine cfRNA concentration (pg/mL) measured by qPCR in paired samples processed immediately ($n = 3$) or after one freeze-thaw cycle ($n = 3$). Comparison was performed using two-sided paired Student's t test. **j**, Volcano plot of genes differentially expressed between urine processed immediately or after one freeze-thaw cycle. **k**, cfRNA concentration (pg/mL) in urine collected into empty urine collection cups and processed at various time points after collection ($n = 3$ biological replicates). Comparison was performed using paired Student's t test using time = 0 as reference. **l**, Volcano plot of genes differentially expressed between urine processed immediately and at 48 hours post collection. **m**, Cell-type composition of paired BLCA urine cfRNA versus sediment ($n = 3$) obtained using CIBERSORTx[60] deconvolution. **n**, Expression of gene signatures overexpressed in normal tissues in 47 healthy control plasma cfRNA samples ($n = 11$ female and $n = 36$ male). **o**, GSEA using cell type-specific gene sets in urine sediment and cfRNA ($n = 3$ paired urine samples). Cell type enriched signatures were selected as defined in Methods. **p**, GSEA using cell type-specific gene sets in plasma cfRNA ($n = 3$) vs urine cfRNA ($n = 3$). In box plots, the center line denotes the median, the box contains the interquartile range (IQR), and the whiskers extend to 1.5 × IQR. Panel **a** created in BioRender; Shi, W. https://biorender.com/kk01zkl (2026).

https://doi.org/10.1038/s41591-026-04673-3



Extended Data Fig. 2 | Identification and characterization of urine rare abundance genes. a, Plot of Log_2 normalized expression (Log_2NX) and percent of samples with gene expressed in 38 reference urine cfRNA. Dotted line indicates the threshold used for defining urine Rare Abundance Genes (uRAGs) ($Log_2NX < 0$ and expressed in < 20% of reference urine cfRNA). Red dots indicate the 3,834 uRAGs and all other genes are shown in grey. **b**, Plot of Log_2NX and Gini Coefficient of gene expression in reference urine cfRNA ($n = 38$). Highlighted are 50 housekeeping genes included in the uRAG selector. **c**, Schematic depicting genes included in the core modules of uRAGs capture panel and examples of optional add-on modules that could be used to supplement uRAGs. In total, the uRAG-focused panel used in this study includes 4,782 genes. **d**, Comparison of expression of shared genes with all exons captured between whole-coding transcriptome panel and uRAG panel in 38 reference urine cfRNA samples. The uRAG genes are highlighted in red. Pearson Correlation is shown. $P \leq 2.2x10^{-16}$. **e**, Comparison of the number of genes detected among shared genes in uRARE-seq libraries captured with both the whole-coding transcriptome and uRAG capture panels ($n = 38$). Threshold for detection is one or more unique reads. Sequencing data were down sampled to achieve equivalent sequencing depth in all samples. Comparison was performed using two-sided paired Student's t-test. **** $P = 1.74e\text{-}07$. In box plots, the center line denotes the median, the box contains the interquartile range (IQR), and the whiskers extend to 1.5 × IQR.

https://doi.org/10.1038/s41591-026-04673-3

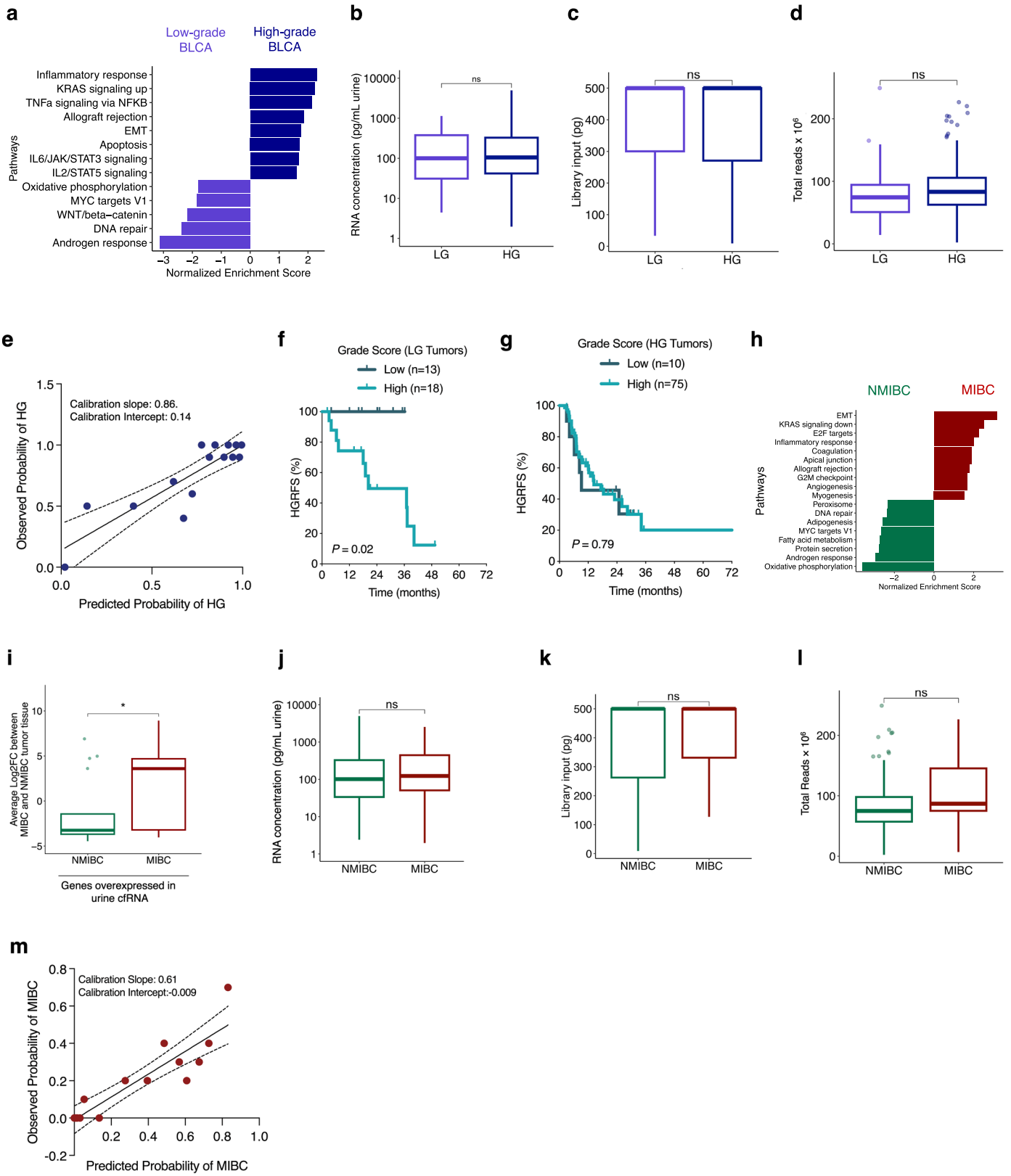


Extended Data Fig. 3 | See next page for caption.

https://doi.org/10.1038/s41591-026-04673-3

Extended Data Fig. 3 | BLCA detection using uRARE-seq. a,**b**,**c**, Key metrics for healthy control urine cfRNA (*n* = 100) and BLCA urine (*n* = 151) cfRNA samples used for BLCA Detection Model training, **a**, Concentration of urine cfRNA quantified by qPCR. **b**, RNA input into library preparation. **c**, total sequencing depth. Comparisons were performed using two-sided Student's t-test. **d**, Average $\log_2$ fold change between BLCA tumor tissue and normal urothelium of the genes enriched in either control (*n* = 100) or BLCA urine cfRNA (*n* = 151). **e**, Schematic of BLCA Detection Model training and validation. **f**, Sensitivity of detection using BLCA Detection Model stratified by library input of 0–100 pg (*n = 15)*, 100–200 pg (*n = 11)*, 200–300 pg (*n = 14)*, *30*0–400 pg (*n = 10)*, *40*0–500 pg (*n = 101)*. Error bars represent 95% binomial confidence interval. Comparison was performed using Kruskal-Wallis. **g**, Detection rate in male and female control and BLCA urine samples. Comparisons were performed using two-sided Fisher's exact test. **h**, Heatmap showing pairwise Pearson correlation between 20 technical replicates from 10 BLCA patients. **i**, Heatmap showing pairwise Pearson correlation between 21 technical replicates from 10 non-cancer controls. **j**, Scattered plot of BLCA Detection Score among technical replicates from control (n=10) and BLCA (n=10) patients. **k**, Relationship between BLCA Detection scores in the same technical replicates. **l**, Analysis of the effect of control (*n = 100)* and BLCA (*n = 151)* samples used for BLCA Detection Model training. Dotted line represents AUC of the full uRARE-seq Detection Model. Data are presented as median values +/− SD of AUCs in the 10-folds used for training. **m**, Percent of patients detected by uRARE-seq BLCA Detection Model or urine cytology in samples with both available (*n* = 93) stratified by grade and stage. **n**, Detection rate in controls with benign urologic conditions among non-cancer control subjects included in our study. *P* values are calculated using two-sided Fisher's exact test. In box plots, the center line denotes the median, the box contains the interquartile range (IQR), and the whiskers extend to 1.5 × IQR. Panel **e** created in BioRender; Shi, W. https://biorender.com/5cgw1nn (2026).

https://doi.org/10.1038/s41591-026-04673-3

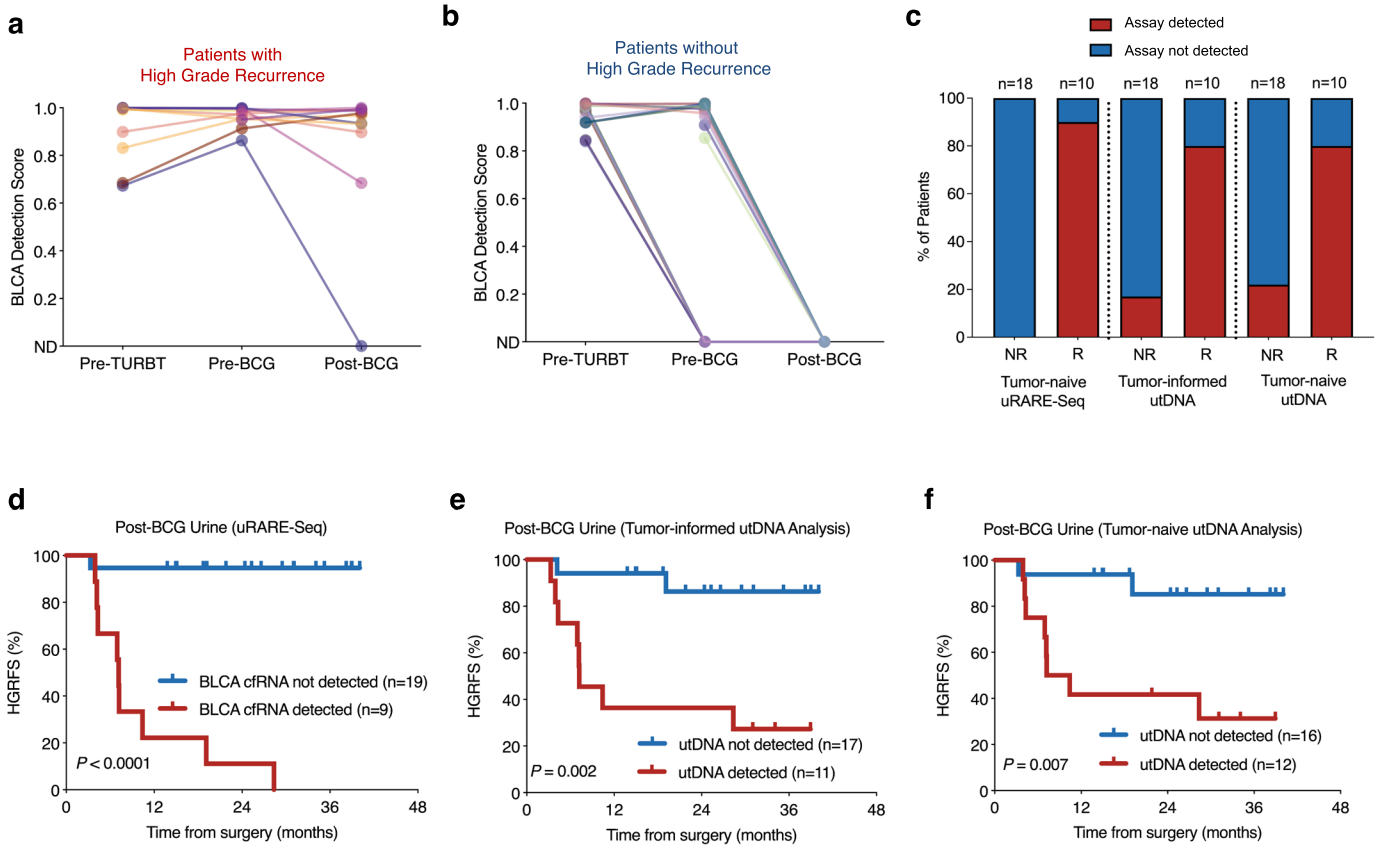


Extended Data Fig. 4 | See next page for caption.

https://doi.org/10.1038/s41591-026-04673-3

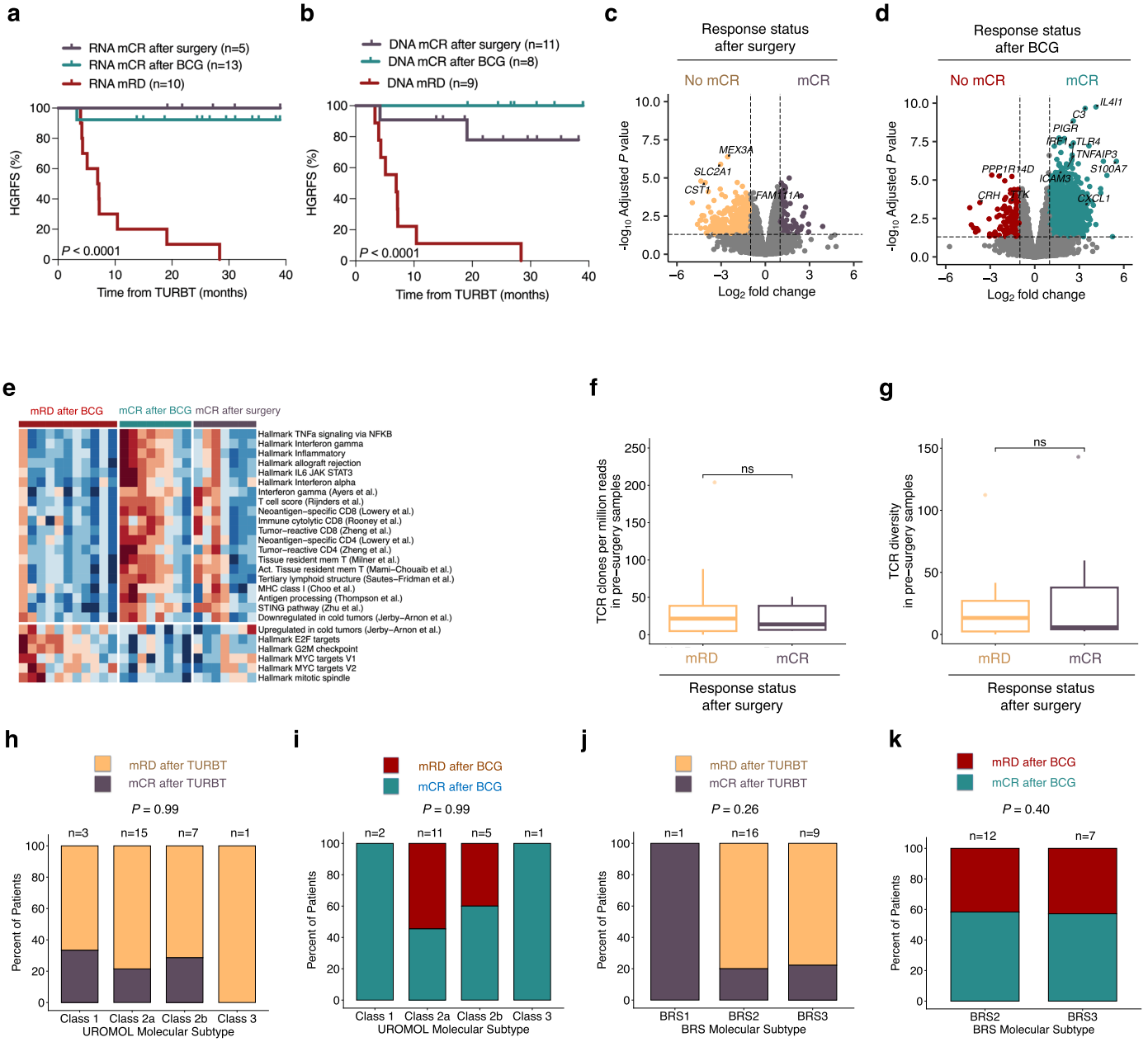
Extended Data Fig. 4 | Urine-based detection of BLCA grade and invasiveness. **a**, Hallmark gene set GSEA of low-grade (LG; $n = 31$) versus high-grade (HG; $n = 113$) BLCA urine cfRNA. **b**,**c**,**d**, Sample level metrics for LG ($n = 31$) and HG ($n = 113$) BLCA urine cfRNA samples used for BLCA Grade Model training. Comparisons were performed using two-sided Student's t-test. **b**, Concentration of urine cfRNA quantified by qPCR. **c**, RNA input mass into library preparation. **d**, sequencing depth. **e**, Calibration analysis of observed probability of HG versus BLCA Grade Model's predicted probability of HG. Each circle represents a group of 10 BLCA urine samples. **f**,**g**, Kaplan-Meier analysis of high-grade recurrence-free survival (HGRFS) stratified by BLCA Grade Model score in **f**, LG tumors ($n = 31$) and **g**, HG tumor samples ($n = 85$). Statistical significance was assessed using a two-sided log-rank test. The cutpoint was determined using R package survminer in LG tumors (0.446). **h**, Hallmark gene set GSEA of NMIBC ($n = 116$) and MIBC ($n = 28$) urine cfRNA. **i**, Genes differentially expressed in urine cfRNA from patients with NMIBC versus MIBC are also differentially expressed in tumor tissue. Comparison was performed using two-sided Student's t-test. * P = 0.001. **j**,**k**,**l**, Sample level metrics of NMIBC ($n = 116$) and MIBC ($n = 28$) urine cfRNA samples used for training the BLCA Muscle Invasion Model. Comparisons were performed using two-sided Student's t-test. **j**, Concentration of urine cfRNA after extraction quantified by qPCR **k**, RNA inputted into library prep **l**, total sequencing depth. **m**, Calibration analysis of observed probability of MIBC versus BLCA Muscle Invasion Model's predicted probability of MIBC in the training cohort. Each circle represents a group of 10 BLCA urine samples. In box plots, the center line denotes the median, the box contains the interquartile range (IQR), and the whiskers extend to 1.5 × IQR.

https://doi.org/10.1038/s41591-026-04673-3



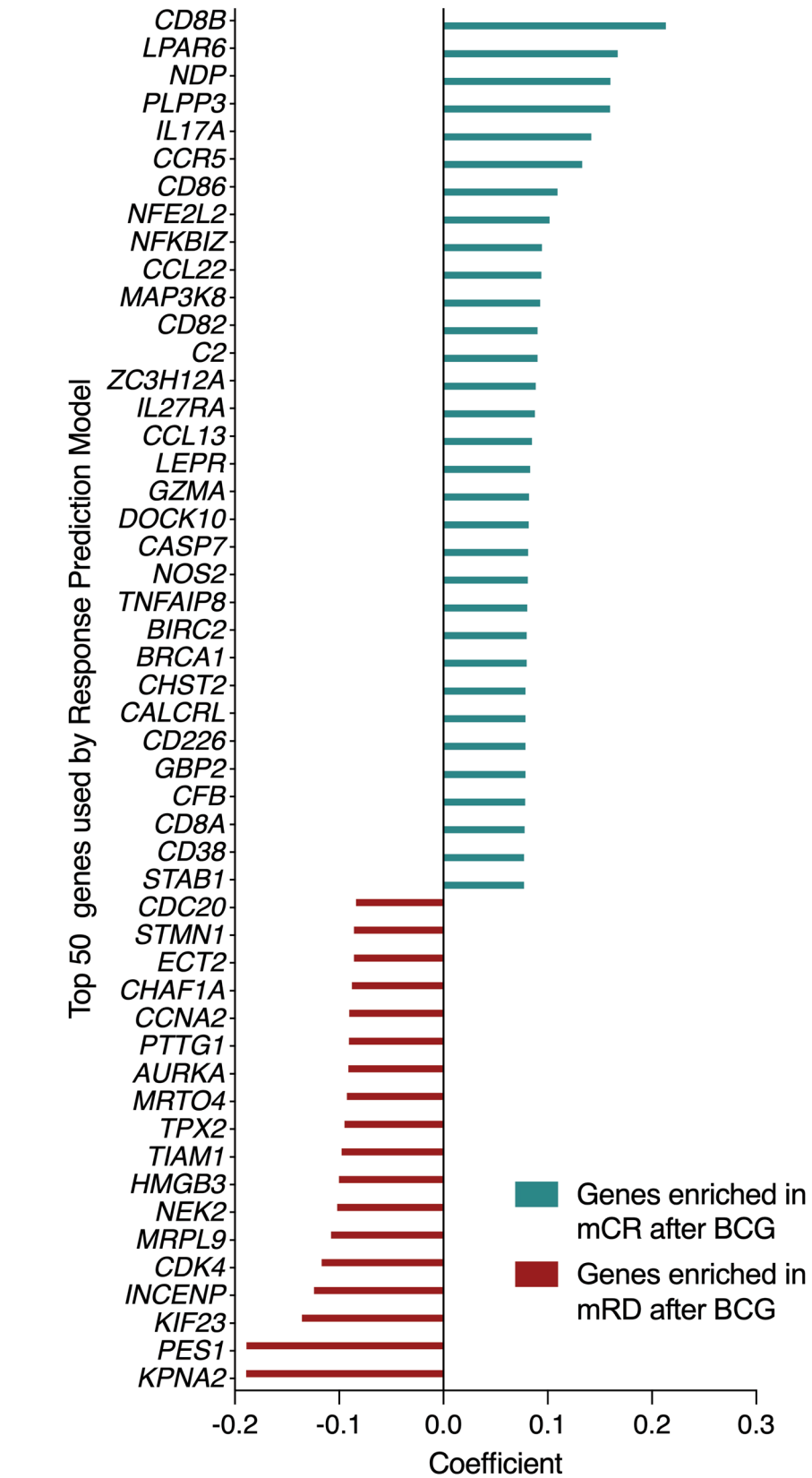
Extended Data Fig. 5 | Minimal residual disease detection in NMIBC using uRARE-seq. a, Time course analysis of NMIBC patients who developed recurrence ($n = 13$). **b**, Time course analysis of NMIBC patients who did not develop recurrence ($n = 23$). **c**, Relationship between bladder cancer detection and patient outcomes at the post-BCG landmark in patients with both uRARE-Seq and uCAPP-seq data available ($n = 28$). **d**,**e**,**f**, Kaplan-Meier analysis of high-grade recurrence-free survival (HGRFS) in the same cohort stratified by BLCA detection based on **d**, uRARE-seq cfRNA analysis, $P = 6.5e\text{-}06$ **e**, Tumor-informed utDNA analysis using field-effect-informed uCAPP-Seq **f**, Tumor-naive utDNA analysis (n=28). Statistical significance was assessed using two-sided log-rank tests.

https://doi.org/10.1038/s41591-026-04673-3



Extended Data Fig. 6 | Responders to surgery and BCG have distinct cfRNA profiles. a, Kaplan Meier analysis of the subset of BLCA patients who had matched uCAPP-Seq DNA data ($n = 28$) stratified by molecular response based on the uRARE-seq BLCA Detection Model. $P = 1.6e\text{-}06$. **b**, as in a but stratified using uCAPP-Seq utDNA analysis ($n = 28$). Comparison was performed using two-sided Log-rank test. $P = 1.1e\text{-}06$. **c**, Differential gene expression analysis using Pre-surgery urine samples from patients with mRD ($n = 19$) versus mCR after surgery ($n = 7$). Adjusted P values indicate BH multiple hypothesis correction. **d**, Differential gene expression analysis using Pre-surgery urine samples from patients with mRD ($n = 11$) versus mCR after BCG ($n = 8$). Adjusted P values indicate BH multiple hypothesis correction. **e**, Heatmap of urine cfRNA gene expression for previously defined immune and proliferation-related gene signatures in patients with mRD after BCG ($n = 11$), and mCR after BCG ($n = 8$), and mCR after surgery ($n = 7$). **f**, TCR clones per million reads between patients with mRD ($n = 17$) versus with mCR after surgery ($n = 7$). **g**, TCR diversity calculated using inverse Simpson between patients with mRD ($n = 17$) versus with mCR after surgery ($n = 7$). Comparisons were performed using two-sided Mann-Whitney U test. **h**,**i**, Relationship between UROMOL molecular subtype[30] and **h**, surgery response status or **i**, BCG response status using RNA-seq of bulk FFPE tumor samples. Comparisons were performed using two-sided Fisher Exact Test. **j**,**k**, Relationship between BRS molecular subtype and **j**, surgery response status or **k**, BCG response status using RNA-Seq of bulk FFPE tumor samples. UROMOL and BRS classes were determined using RNA-seq of FFPE tumor tissue. Comparisons were performed using two-sided Fisher Exact Test. In box plots, the center line denotes the median, the box contains the interquartile range (IQR), and the whiskers extend to 1.5 × IQR.

https://doi.org/10.1038/s41591-026-04673-3



Extended Data Fig. 7 | Top genes used by the Response Prediction Model. a, Top 50 genes used by the Response Prediction Model.

https://doi.org/10.1038/s41591-026-04673-3

Extended Data Table 1 | Summarized demographics of urine samples used for cancer detection

	Controls			BLCA		
	Training	Validation	P value	Training	Validation	P value
No. of Samples	100	140		151	142	
No. of donors	98	140		140	137	
Sex			$P = 0.65$			$P = 0.25$
Male	74 (74%)	108 (77%)		132 (87%)	117 (82%)	
Female	26 (26%)	32 (23%)		19 (13%)	25 (18%)	
Median Age (years)	61(23-96)	67 (20-93)		75 (29-94)	75 (27-100)	
Control Population						
Healthy Controls	48 (48%)	37 (26%)		NA	NA	
LUTS/Hematuria	52 (52%)	103 (74%)		NA	NA	
Smoking			$P = 0.19$			$P = 0.37$
Current/Former	39 (39%)	67 (48%)		110 (73%)	92 (65%)	
Never	61 (61%)	73 (52%)		40 (27%)	48 (34%)	
Unknown	0 (0%)	0 (0%)		1 (0%)	2 (1%)	
Stage						
CIS	NA	NA		13 (9%)	23 (16%)	
Ta	NA	NA		76 (50%)	60 (42%)	
T1	NA	NA		34 (23%)	29 (21%)	
T2	NA	NA		28 (18%)	30 (21%)	
Grade						$P = 0.89$
LG	NA	NA		36 (24%)	32 (23%)	
HG	NA	NA		115 (76%)	110 (77%)	
Institution						
Stanford	58 (58%)	60 (43%)		55 (36%)	82 (58%)	
VA	42 (42%)	80 (57%)		96 (64%)	60 (42%)	

nature portfolio

Corresponding author(s): Maximilian Diehn, Joseph Liao, Ash Alizadeh

Last updated by author(s): Jul 28, 2026

Reporting Summary

Nature Portfolio wishes to improve the reproducibility of the work that we publish. This form provides structure for consistency and transparency in reporting. For further information on Nature Portfolio policies, see our Editorial Policies and the Editorial Policy Checklist.

Statistics

For all statistical analyses, confirm that the following items are present in the figure legend, table legend, main text, or Methods section.

n/a	Confirmed	
☐	☒	The exact sample size (*n*) for each experimental group/condition, given as a discrete number and unit of measurement
☐	☒	A statement on whether measurements were taken from distinct samples or whether the same sample was measured repeatedly
☐	☒	The statistical test(s) used AND whether they are one- or two-sided *Only common tests should be described solely by name; describe more complex techniques in the Methods section.*
☐	☒	A description of all covariates tested
☐	☒	A description of any assumptions or corrections, such as tests of normality and adjustment for multiple comparisons
☐	☒	A full description of the statistical parameters including central tendency (e.g. means) or other basic estimates (e.g. regression coefficient) AND variation (e.g. standard deviation) or associated estimates of uncertainty (e.g. confidence intervals)
☐	☒	For null hypothesis testing, the test statistic (e.g. *F*, *t*, *r*) with confidence intervals, effect sizes, degrees of freedom and *P* value noted *Give P values as exact values whenever suitable.*
☒	☐	For Bayesian analysis, information on the choice of priors and Markov chain Monte Carlo settings
☒	☐	For hierarchical and complex designs, identification of the appropriate level for tests and full reporting of outcomes
☐	☒	Estimates of effect sizes (e.g. Cohen's *d*, Pearson's *r*), indicating how they were calculated

Our web collection on statistics for biologists contains articles on many of the points above.

Software and code

Policy information about availability of computer code

Data collection	Data processing was performned using fastp (v0.20.0), STAR (v2.7.0), RSEM (v1.2.28), RNASeQC (v2.3.5), samtools (v1.11).
Data analysis	Data analysis was performed using R (v4.1.3) or prism (v10). Expression normalization was done using the R packages tximport (v1.22) and edge R (v3.36). Differential expression analyses used the R packages DESeq2 (v1.34) and fgsea (v1.20). Machine learning models were performed using python (v3.13.7) and scikit-learn (v1.6.1).

For manuscripts utilizing custom algorithms or software that are central to the research but not yet described in published literature, software must be made available to editors and reviewers. We strongly encourage code deposition in a community repository (e.g. GitHub). See the Nature Portfolio guidelines for submitting code & software for further information.

Data

Policy information about availability of data

All manuscripts must include a data availability statement. This statement should provide the following information, where applicable:

- Accession codes, unique identifiers, or web links for publicly available datasets
- A description of any restrictions on data availability
- For clinical datasets or third party data, please ensure that the statement adheres to our policy

De-identified clinical and demographic data for individuals included in this study as well as model scores and other data are provided in the Supplementary Tables. Gene expression data from GTEx and TCGA were retrieved from the UCSC Xena Repository. Gene expression data from the UROMOL BLCA study were obtained

from Lindskrog et al (EGAS00001004693). Cell type marker gene lists were downloaded from the PanglaoDB resource (https://panglaodb.se/markers.html). Custom gene signatures were generated using the Tabula Sapiens gene expression data. Interferon gamma and T cell gene lists were obtained from Ayers et al. and Rijnders et al, respectively. The RNA sequencing data generated in this study is available in dbGaP (phs004116). The bioinformatic codes used for various classifiers is available on https://github.com/kevinjliustanford/uRARESeq. Requests for additional information should be addressed to M.D.

Research involving human participants, their data, or biological material

Policy information about studies with human participants or human data. See also policy information about sex, gender (identity/presentation), and sexual orientation and race, ethnicity and racism.

Reporting on sex and gender	This study includes both male and female participants and sex was self-reported and identified from medical records. Summarized sex statistics is in Extended Data Table 1 and clinical and demographic characteristics usch as age, sex, and smoking history of all participants in the study can be found in Supplemental Table 1. Our cohort consist of approximately ~74-77% male and ~23-26% female samples in the control cohort and ~82-87% male and ~13-18% female samples in the BLCA cohort. The sex ratio observed in this study is consistent with the sex prevalence of bladder cancer. Sex was considered as part of experimental design. Both males and females were eligible to participate. To minimize the risk of our machine learning-based biomarkers being impacted by sex, we removed genes with sex-specific expression differences as potential features
Reporting on race, ethnicity, or other socially relevant groupings	Social relevant grouping were not collected in this study.
Population characteristics	For the control cohort, the median age of the training cohort was 61 (range 23-96) and 67 in the validation cohort (range 20-93). For the bladder cancer cohort, the median age of the training cohort was 75 (range 29-94) and 75(range 27-100) in the validation cohort. Our cohort consist of approximately ~72-74% male and ~26-28% female control samples and ~82-87% male and ~13-18% female samples in the cancer cohort. Summarized sex statistics is in Extended Data Table 1 and clinical and demographic characteristics usch as age, sex, and smoking history of all participants in the study can be found in Supplemental Table 1.
Recruitment	Patients were recruited based on confirmed diagnosis of bladder cancer, prostate cancer, renal cell carcinoma, or based on negative pathology findings from urine cystoscopy. All participants provided written informed consent for the use of their clinical data and biospecimens for research using protocols approved by Institutional Review Boards at their respective centers. Collection centers included Stanford University and VA Palo Alto. Participants were not compensated for this study.
Ethics oversight	All participants provided written informed consent for the use of their clinical data and biospecimens for research and approved by Institutional Review Boards at their respective centers. Collection centers included Stanford University and VA Palo Alto.

Note that full information on the approval of the study protocol must also be provided in the manuscript.

Field-specific reporting

Please select the one below that is the best fit for your research. If you are not sure, read the appropriate sections before making your selection.

☒ Life sciences ☐ Behavioural & social sciences ☐ Ecological, evolutionary & environmental sciences

For a reference copy of the document with all sections, see nature.com/documents/nr-reporting-summary-flat.pdf

Life sciences study design

All studies must disclose on these points even when the disclosure is negative.

Sample size	Sample cohort sizes were determined by sample availability, so no statistical calculations were performed to determine cohort size prior to patient enrollment
Data exclusions	No data were excluded in this study
Replication	Technical experiments performed in this study were validated in n=3 biological samples. In addition, the study findings were validated in an independent validation cohort
Randomization	Randomization was not applicable in this study because all samples were assigned based on confirmed diagnosis of bladder cancer, prostate cancer, kidney cancer, or non-cancer based on negative cystoscopy results.
Blinding	Blinding was not performed in this study because this was not necessary for this observational study for the purpose of method development and proof-of-concept data

Reporting for specific materials, systems and methods

We require information from authors about some types of materials, experimental systems and methods used in many studies. Here, indicate whether each material, system or method listed is relevant to your study. If you are not sure if a list item applies to your research, read the appropriate section before selecting a response.

Materials & experimental systems

n/a	Involved in the study
☒	☐ Antibodies
☒	☐ Eukaryotic cell lines
☒	☐ Palaeontology and archaeology
☒	☐ Animals and other organisms
☒	☐ Clinical data
☒	☐ Dual use research of concern
☒	☐ Plants

Methods

n/a	Involved in the study
☒	☐ ChIP-seq
☒	☐ Flow cytometry
☒	☐ MRI-based neuroimaging

Plants

Seed stocks

Report on the source of all seed stocks or other plant material used. If applicable, state the seed stock centre and catalogue number. If plant specimens were collected from the field, describe the collection location, date and sampling procedures.

Novel plant genotypes

Describe the methods by which all novel plant genotypes were produced. This includes those generated by transgenic approaches, gene editing, chemical/radiation-based mutagenesis and hybridization. For transgenic lines, describe the transformation method, the number of independent lines analyzed and the generation upon which experiments were performed. For gene-edited lines, describe the editor used, the endogenous sequence targeted for editing, the targeting guide RNA sequence (if applicable) and how the editor was applied.

Authentication

Describe any authentication procedures for each seed stock used or novel genotype generated. Describe any experiments used to assess the effect of a mutation and, where applicable, how potential secondary effects (e.g. second site T-DNA insertions, mosiacism, off-target gene editing) were examined.